Electronic Supplementary Information for,

A broad view at the complexity involved in water oxidation catalysis based on Ru-bpn complexes

Abolfazl Ghaderian,[1,2] Alicja Franke,[3] Marcos Gil-Sepulcre,[1] Jordi Benet-Buchholz,[1] Antoni Llobet,[1,4*] Ivana Ivanovic´-Burmazovic´,[3,5*] Carolina Gimbert-Suriñach,[1*]

[1] Institute of Chemical Research of Catalonia (ICIQ), Barcelona Institute of Science and Technology, Av. Països Catalans 16, 43007 Tarragona, Spain.

[2] Departament de Química Física i Inorganica, Universitat Rovira i Virgili, Campus Sescelades, C/Marcel`·lí Domingo, s/n, 43007 Tarragona, Spain

[3] Department of Chemistry and Pharmacy, Friedrich-Alexander University Erlangen-Nuremberg, 91058 Erlangen, Germany

[4] Universitat Autònoma de Barcelona, Departament de Química, Cerdanyola del Vallès, 08193 Barcelona, Spain

[5] Department Chemie, Ludwigs-Maximilians-Universität, Butenandtstraße 5–13, 81377 München, Germany

Table of Content

Spectroscopy

Nuclear Magnetic Resonance (NMR)

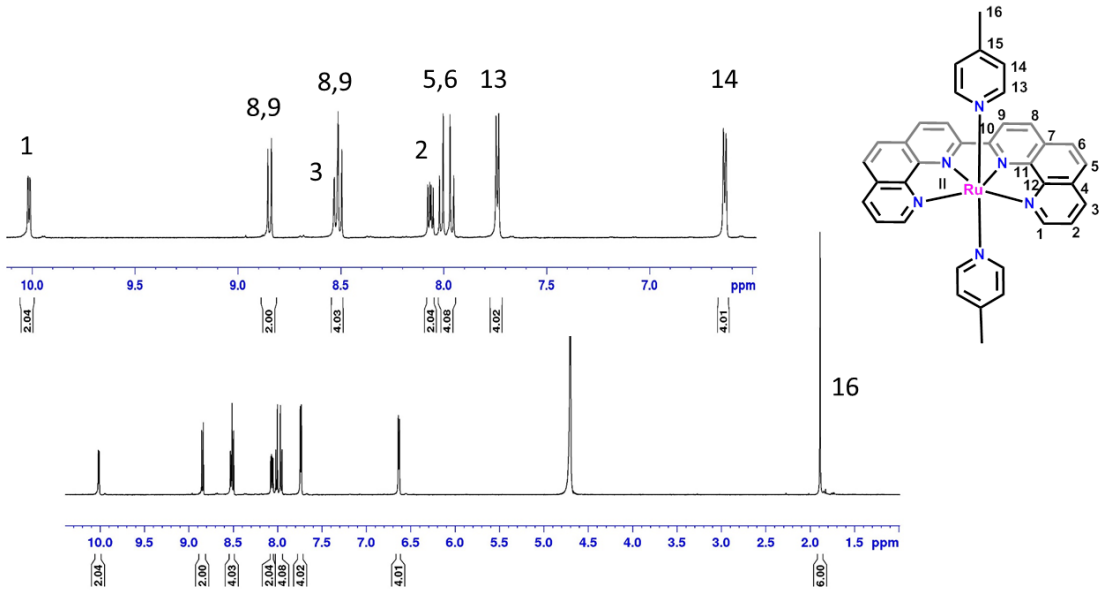

Figure S1. ^{1}H-NMR spectrum of $\mathbf{1}^{2+}$ in D_2O at T= 298K. Inset, enlargement of aromatic region.

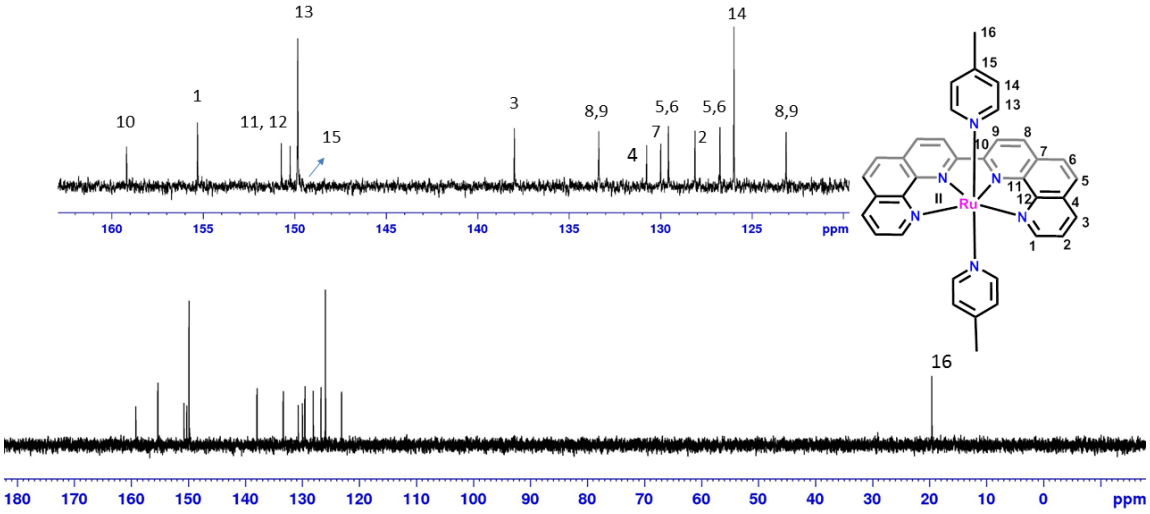

Figure S2. ^{13}C{H} NMR of $\mathbf{1}^{2+}$ in D_2O at T= 298K. Inset, enlargement of aromatic

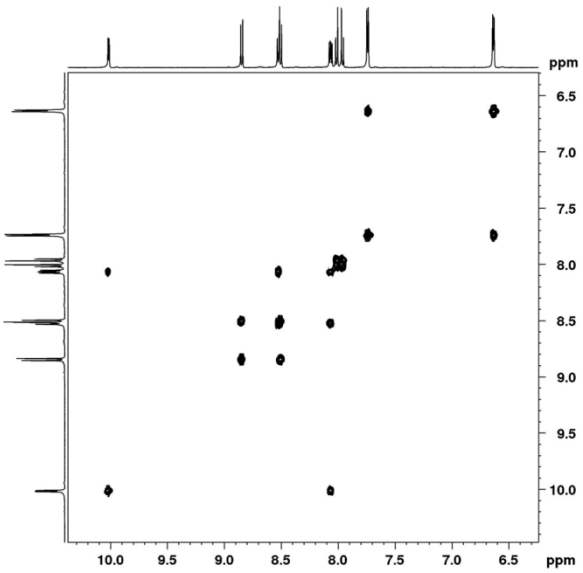

Figure S3. ^{1}H-^{1}H COSY of $\mathbf{1}^{2+}$ in D_2O at T = 298K.

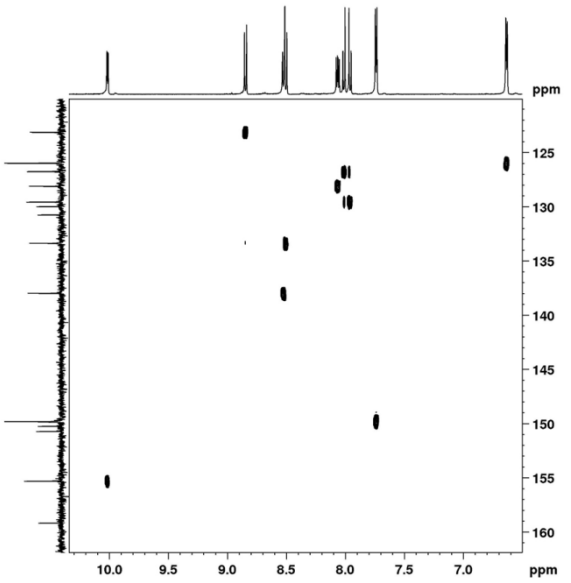

Figure S4. ^{1}H-^{13}C HSQC NMR of $\mathbf{1}^{2+}$ in D_2O at T= 298K.

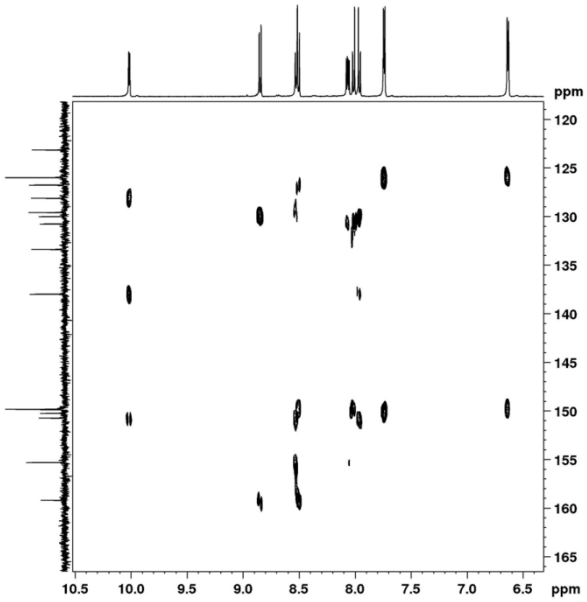

Figure S5. ^{1}H-^{13}C HMBC NMR of $\mathbf{1}^{2+}$ in D_2O at T= 298K.

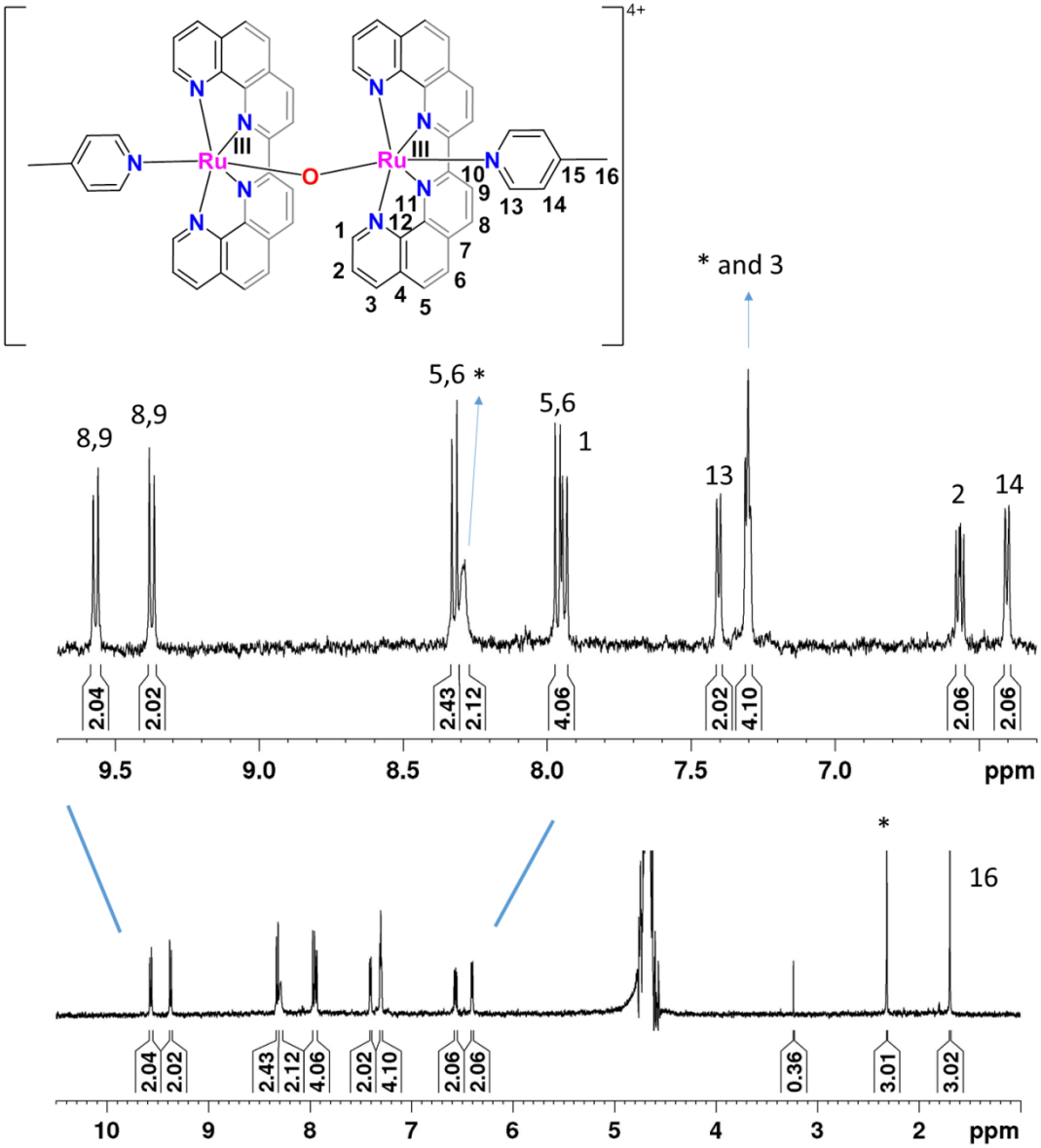

Figure S6. ^{1}H-NMR spectrum of electrochemically generated $\mathbf{3}^{4+}$ from $\mathbf{1}^{2+}$ in a phosphate buffer (phbf) aqueous solution at pD 7 see (Figure S28 for CPE details). Asterisks indicate resonances of free picoline. *Inset*, enlargement of the aromatic region.

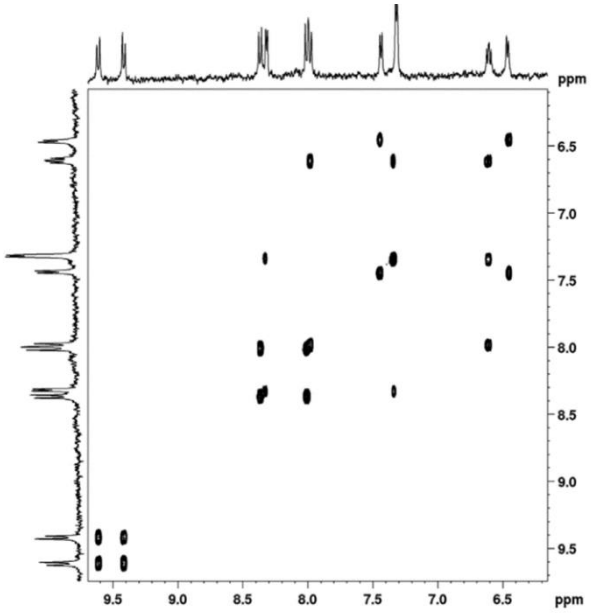

Figure S7. ^{1}H-^{1}H COSY of $\mathbf{3}^{4+}$ in a phbf aqueous solution at pD 7.

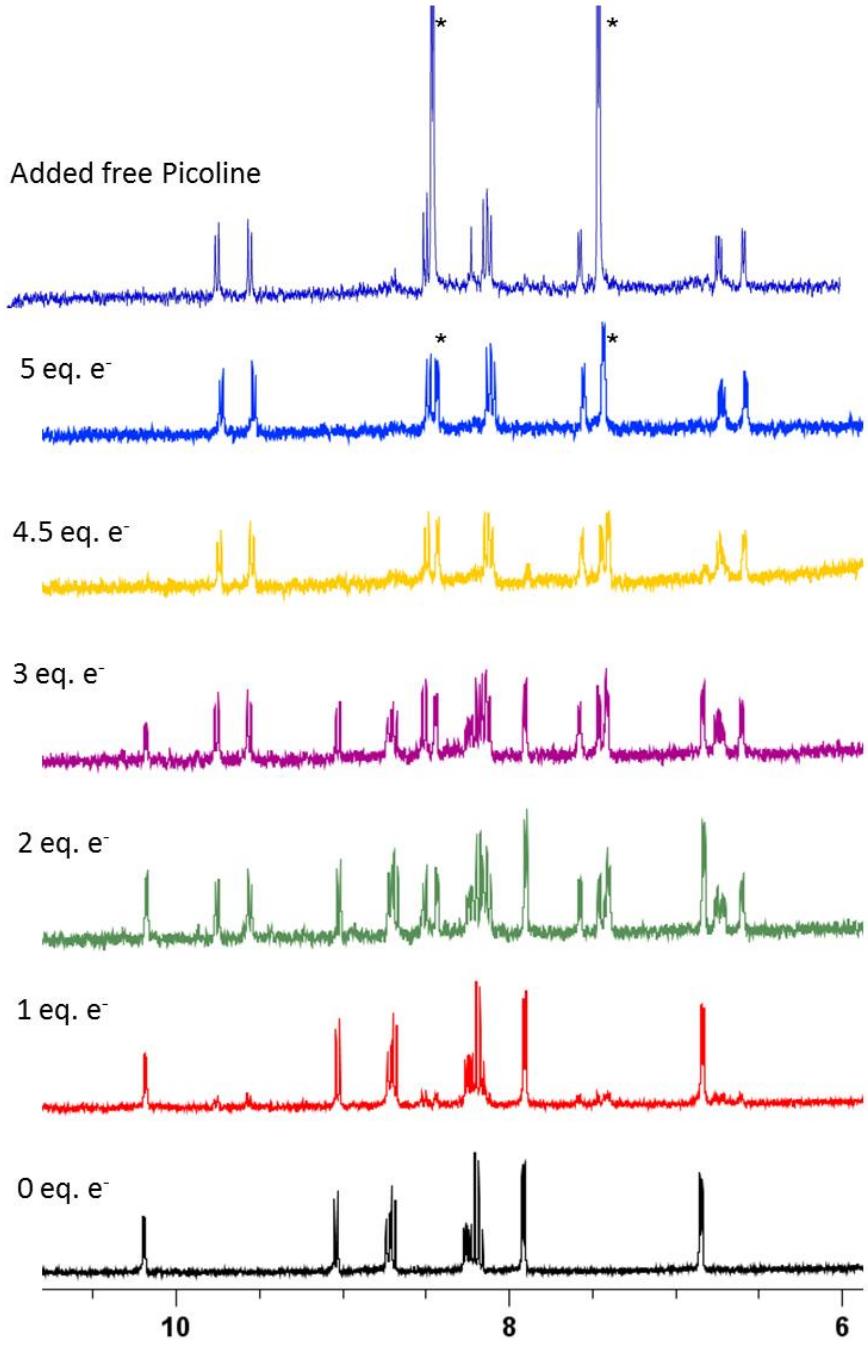

Figure S8. ^{1}H-NMR monitoring of the electrochemical conversion of **1**$^{2+}$ into **3**$^{4+}$ in a phbf solution at pD 7 (see Figure S28 for CPE details). Asterisks indicate resonances of free picoline.

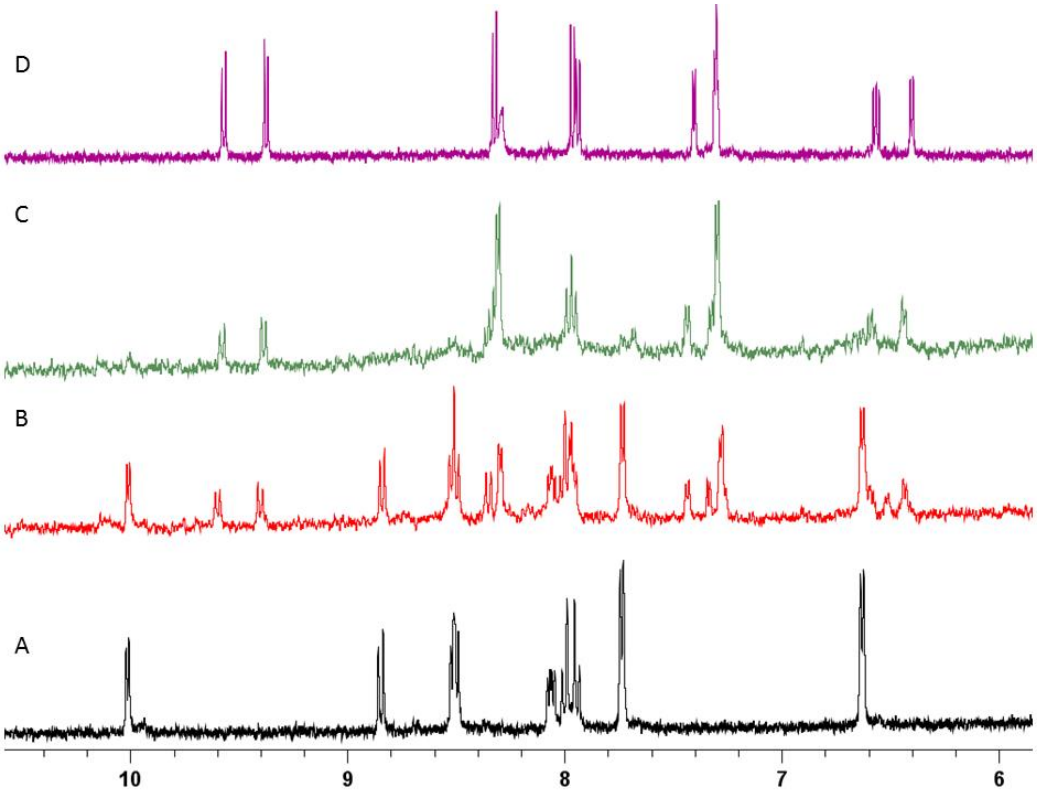

Figure S9. ^{1}H-NMR spectra in a phbf aqueous solution at pD 7 of: A) $\mathbf{1}^{2+}$, B) $\mathbf{1}^{2+}$ + 2 eq. $NaIO_4$, C) $\mathbf{1}^{2+}$ + 4.5 eq. $NaIO_4$ and D) $\mathbf{3}^{4+}$ after CPE at E_{app}=1.45 V vs. NHE.

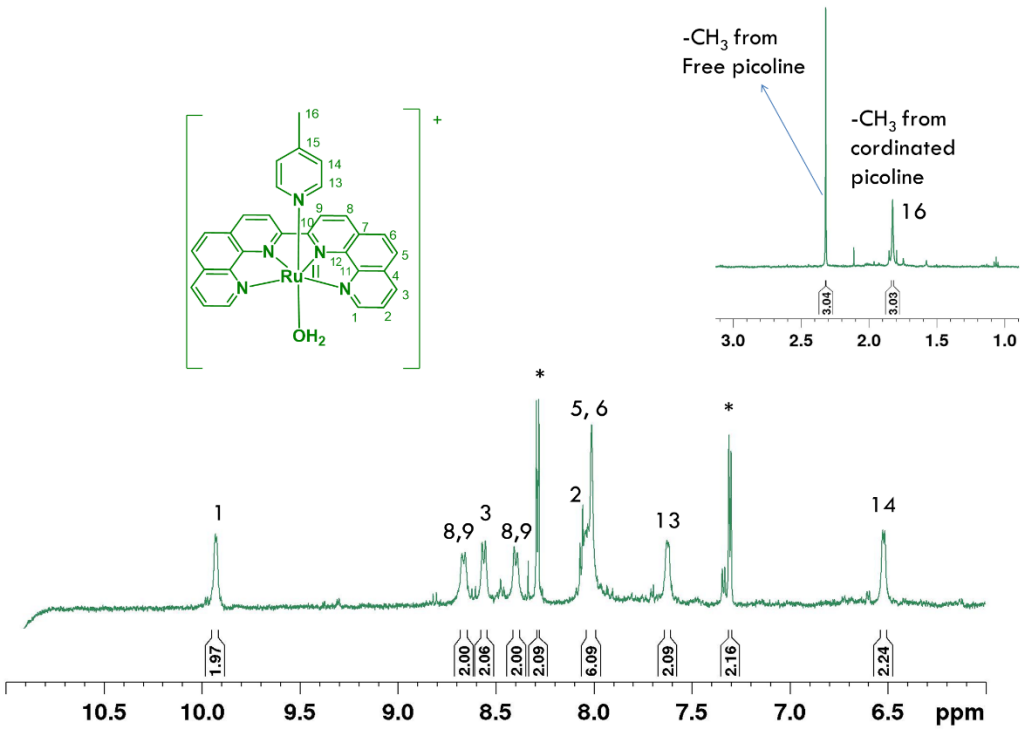

Figure S10. ^{1}H-NMR spectrum of electrochemically generated $\mathbf{4}^{2+}$ from $\mathbf{3}^{4+}$ in a phbf aqueous solution at pD 7 (see Figure S29 for CPE details). Asterisks indicate resonances of free picoline. Inset, enlargement of the aliphatic region.

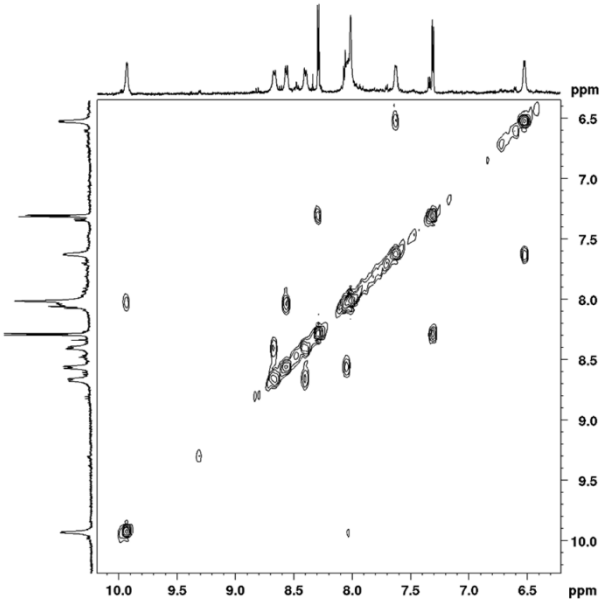

Figure S11. ^{1}H-^{1}H COSY of $\mathbf{4}^{2+}$ at pD 7 at T= 298K.

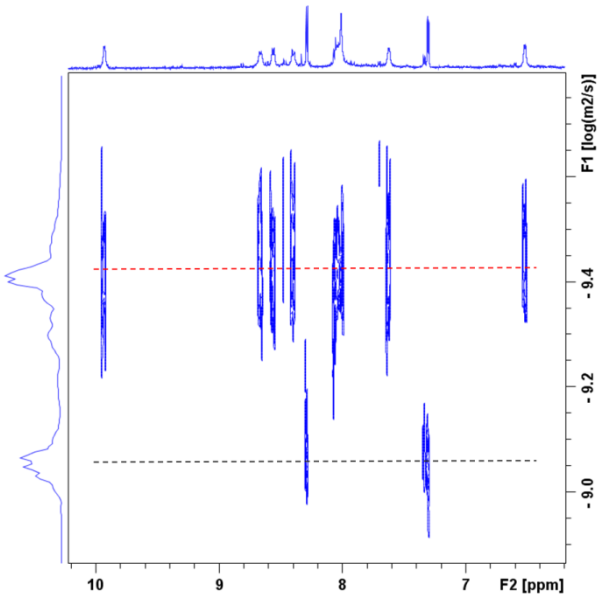

Figure S12. DOSY of $\mathbf{4}^{2+}$ at pD 7. Free picoline appears at *log D* = -9.05.

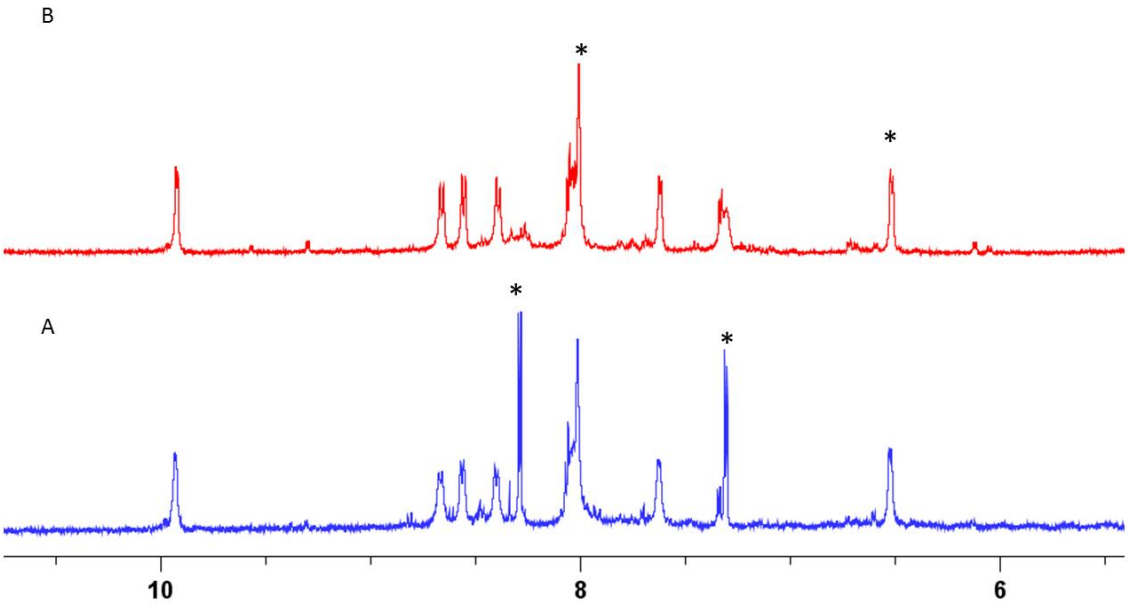

Figure S13. ^{1}H-NMR spectra of electrochemically (CPE at E_{app}= 0.35 in a solution of $\mathbf{3}^{4+}$) A) and chemically (addition of L-ascorbic acid) B), generated $\mathbf{4}^{2+}$ at pD 7. Asterisk indicate resonances of free picoline.

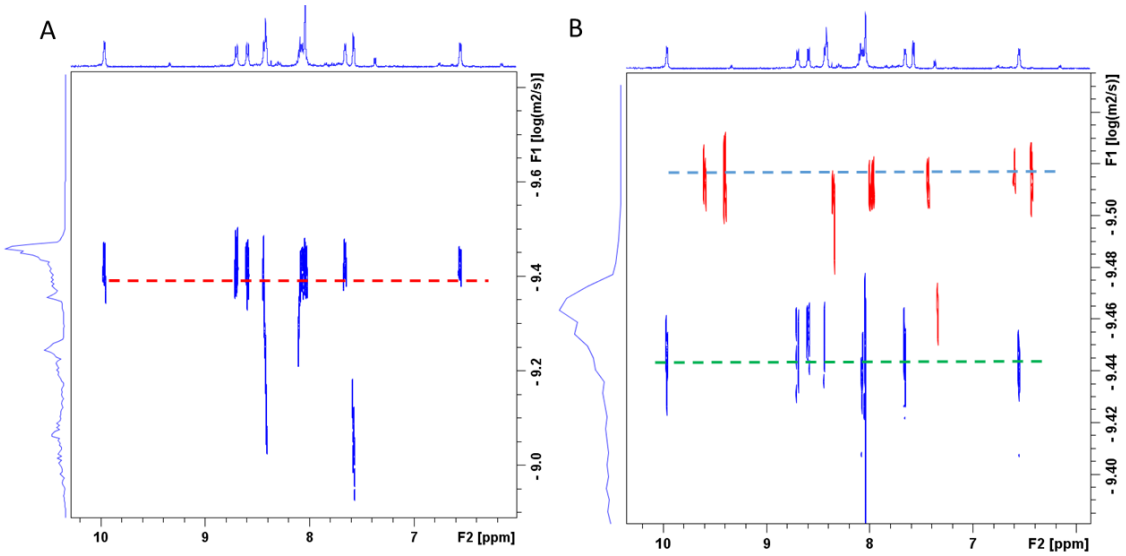

Figure S14. DOSY at pD 7 of: A) $\mathbf{4}^{2+}$ and B) $\mathbf{4}^{2+}$ (blue trace) + $\mathbf{3}^{4+}$ (red trace).

IR Spectroscopy

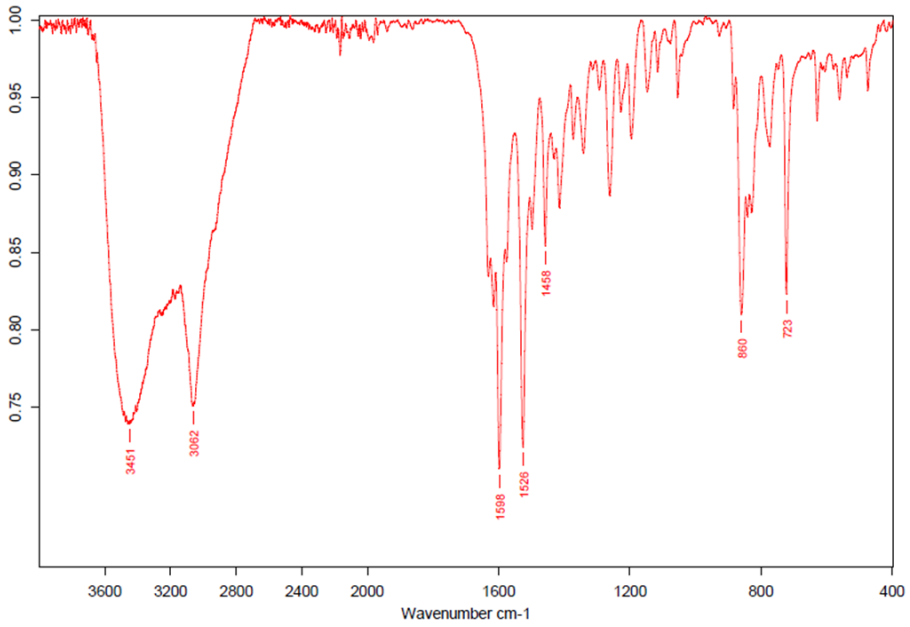

Figure S15. IR spectrum of $[Ru(bpn)(Cl)_2]Cl$.

UV-Vis

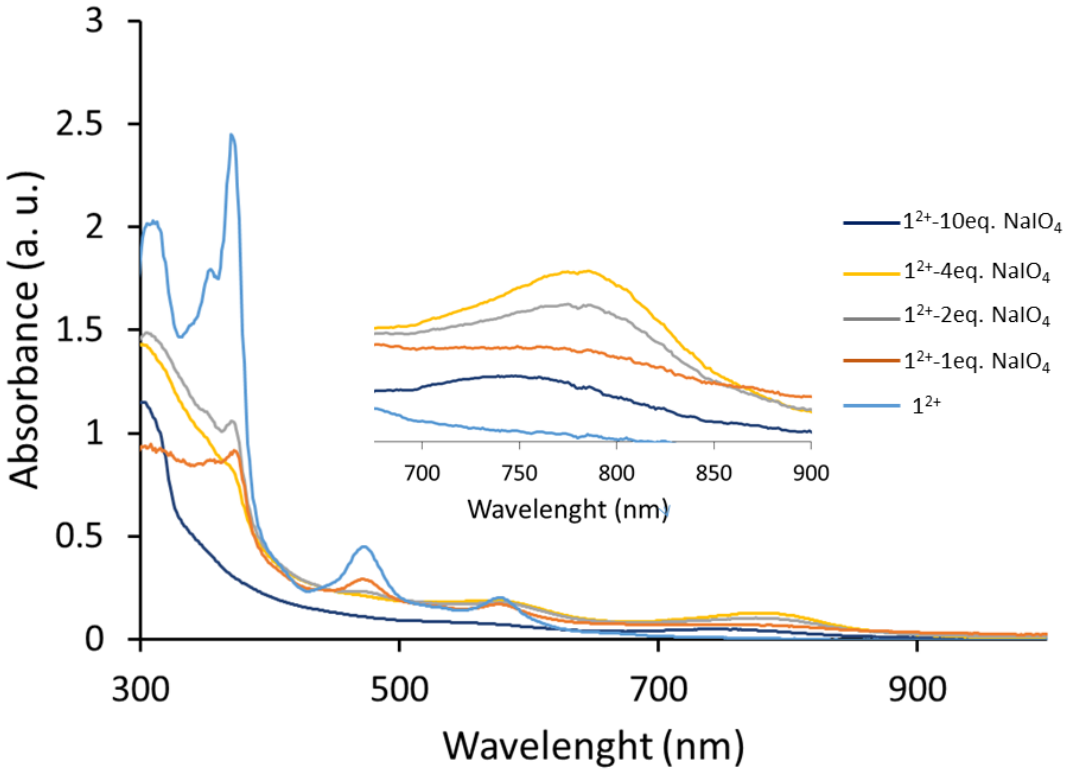

Figure S16. Recorded UV-vis spectra in a solution of $\mathbf{1}^{2+}$ (1mM) after addition of 1 to 10 eq of $NaIO_4$ in a phbf aqueous solution at pH 7. Inset enlargement of the 700-900 nm region.

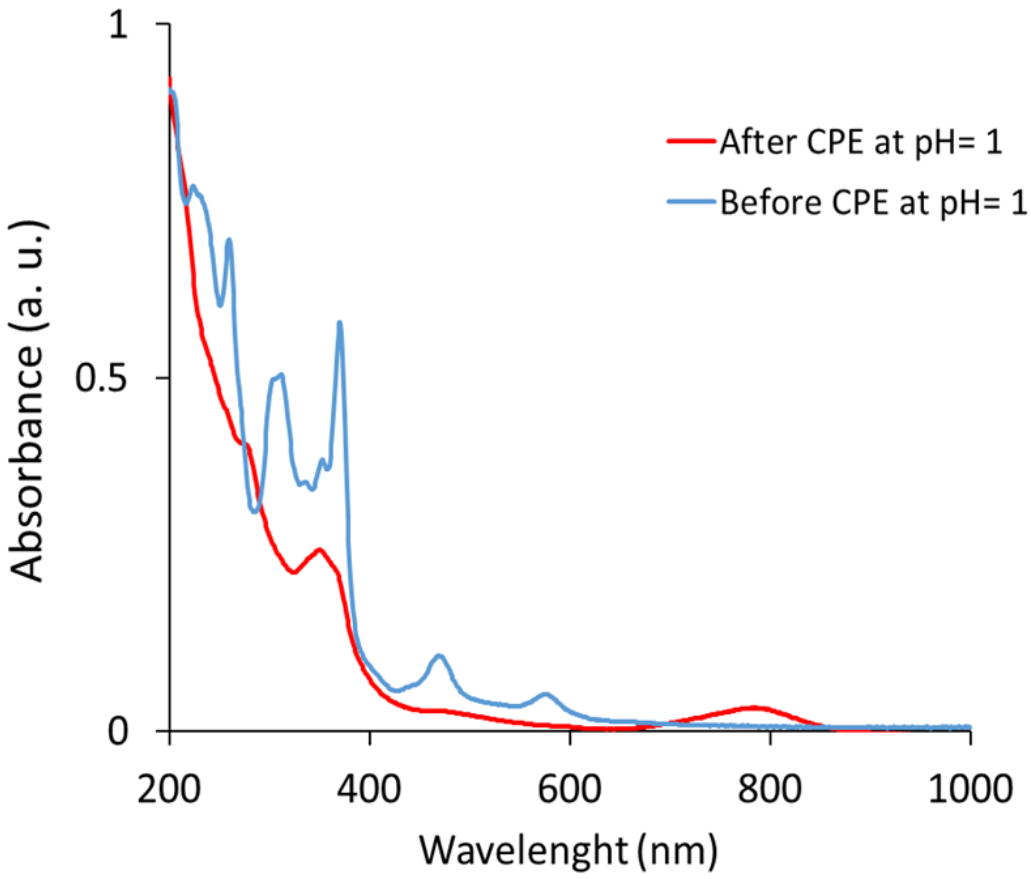

Figure S17. Recorded UV-vis spectra of $\mathbf{1}^{2+}$ (blue color) and new compound (red color) after CPE at E_{app}= 1.65 V in a 1 mM solution of $\mathbf{1}^{2+}$ at pH 1 (TA-TFE (2:1) ([TA]= 0.1 M).

Resonance Raman Spectroscopy

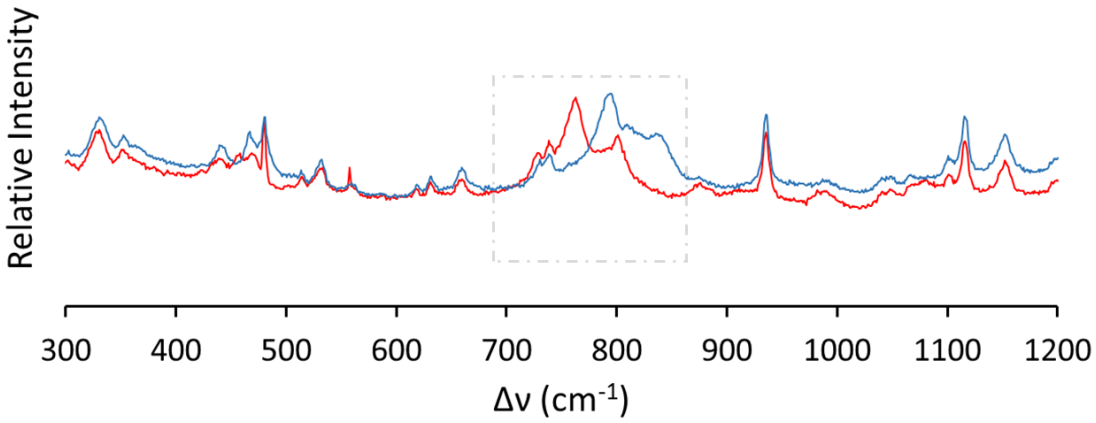

Figure S18. rRaman spectra of an aqueous solution of $\mathbf{3}^{4+}$ prepared *in situ* from $\mathbf{1}^{2+}$ after a CPE electrolysis at E_{app} = 1.45 V at pH 7 phbf solution in H_2O^{16} (blue) and H_2O^{18} (red).

Kinetics and Thermodynamics

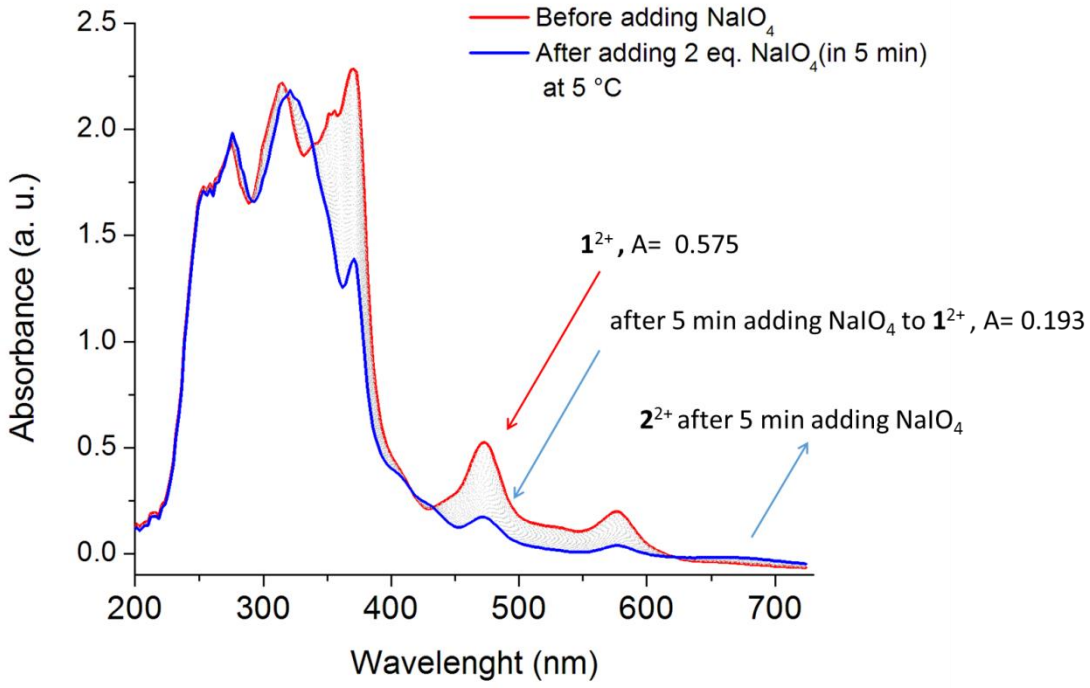

Figure S19. Spectral changes recorded after stopped-flow mixing (1:1 volume ratio, 113 μl of each reagent) of $8x10^{-4}$ mM $NaIO_4$ with $4x10^{-4}$ mM solution of $\mathbf{1}^{2+}$ in phbf at pH 7.2 and 5 °C. 0 min (Red color ($\mathbf{1}^{2+}$)) and 5 min (blue color ($\mathbf{2}^{2+}$)). The gray traces show the spectral changes every 10 seconds.

Table S1. [$NaIO_4$], k_{obs1} with St. deviation (SD) for k_{obs1} and SD for the fits taken from Figure 4C

[$NaIO_4$], M	Mean value of k_{obs1} (s^{-1})	SD of k_{obs1}	SD of fits
8.75×10^{-5}	0.0274	0.00185	$(2.718 – 4.073) \times 10^{-4}$
1.125×10^{-4}	0.0376	0.00435	$(3.370 – 5.147) \times 10^{-4}$
1.50×10^{-4}	0.0452	0.00338	$(3.621 – 4.008) \times 10^{-4}$
2.00×10^{-4}	0.0582	0.00399	$(3.919 – 4.166) \times 10^{-4}$
2.5×10^{-4}	0.0757	0.00713	$(3.994 – 4.132) \times 10^{-4}$

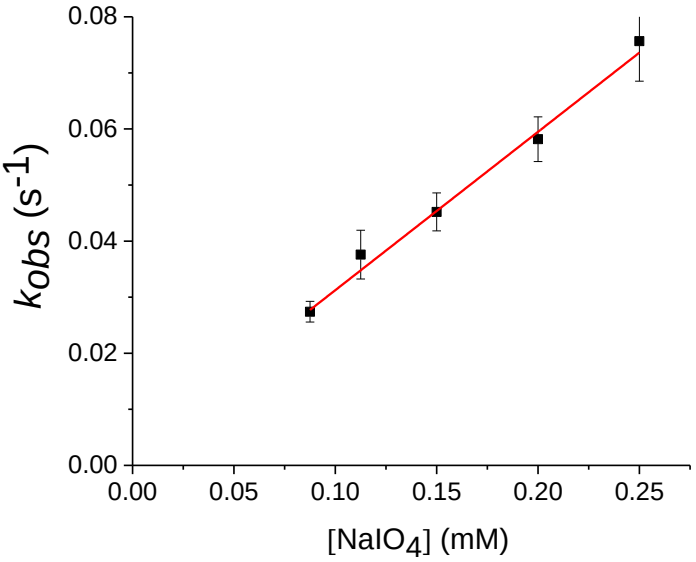

Figure S20. Linear plot of k_{obs1} (s^{-1}) values vs. [$NaIO_4$]. 7–20 equivalent excesses of $NaIO_4$ ([$NaIO_4$] = (0.875 – 2.5) x 10^{-4} M) used over the concentration of $\mathbf{1}^{2+}$ (0.125 x 10^{-4} M) at pH 7.2 phbf solution and 25 °C. The values of k_{obs1} (s^{-1}) were obtained from the experimental data shown in Fig. 4C. The regression parameters to linear function y = ax + b, a = 295.44 ± 10.31, b = 0.0013 ± 0.0016, R^2 = 0.9952.

Table S2. Spectroscopic data for the calculation of [$\mathbf{2}^{2+}$] is taken from Figure S19.

ΔA [$\mathbf{1}^{2+}$]	Ɛ ($\mathbf{1}^{2+}$)	L	[$\mathbf{2}^{2+}$] = ΔA/ƐL
0.382	6472.52 $M^{-1}{\cdot}cm^{-1}$	1 cm	5.9*10^-5 M

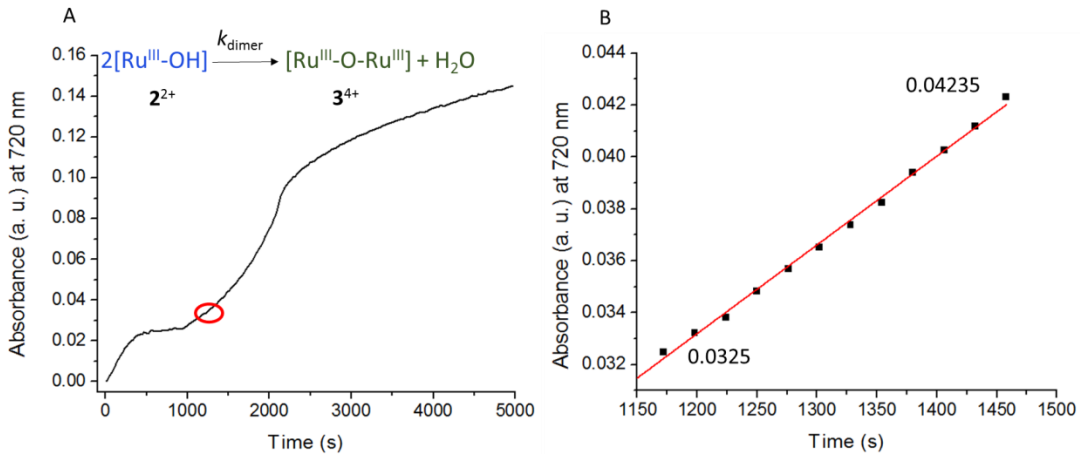

Figure S21. Left, Kinetic traces recorded at 720 nm during 82 min after stopped-flow mixing (1:1 volume ratio, 113 µl of each reagent) of $8x10^{-4}$ mM $NaIO_4$ with $4x10^{-4}$ mM solution of $\mathbf{1}^{2+}$ in phbf at pH 7.2 and 5 °C. Right, enlargement of the 1170-1460 s zone used for the calculation of [$\mathbf{3}^{4+}$]. Fit of experimental data to the linear function y = ax + b; a = 3.419 x $10^{-5} \pm 5.162$ x 10^{-7}; b = -7.8 x $10^{-3} \pm 6.7$ x 10^{-4}; R^2 = 0.9975.

Table S3. Spectroscopic data for the calculation of k_{dimer} for the dimerization reaction (optical path length used, L = 1 mm). The data is taken from Figure S21.

ε($\mathbf{3}^{4+}$)	Slope = ΔC/Δt	$v_{initial}$ = slope/ ε_{dim}.L	[$\mathbf{2}^{2+}$]	k_{dimer}= $v_{initial}$ /[$\mathbf{2}^{2+}$]^2
7281.6 $M^{-1}\cdot cm^{-1}$	(3.42 ± 0.05) x 10^{-5} s^{-1}	(4,696 ± 0.069) x 10^{-9} M s^{-1}	5.9*10^{-5} M	1.349 ± 0.020 M^{-1} s^{-1}

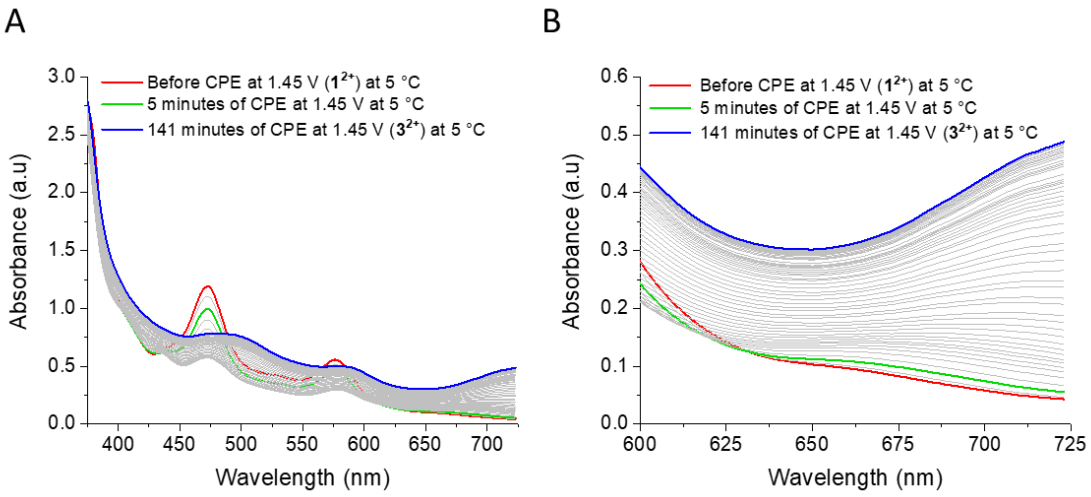

Figure S22. Spectral changes recorded with UV-Vis probe during a CPE at E_{app}= 1.45 V in a phosphate buffer solution at pH 7 (T= 5 ℃), Red ($\mathbf{1}^{2+}$), Green ($\mathbf{2}^{2+}$), Blue ($\mathbf{3}^{4+}$). Conditions: 50 mL of buffered solution (phbf, pH = 7) of $\mathbf{1}^{2+}$ ([$\mathbf{1}^{2+}$] = 0.2 mM, 10 μmol). WE: Pt net electrode (simple cylindrical Pt wire electrode, diameter: 35 mm and cylinder height: 50 mm); CE: Pt wire; RE: silver wire, the potential reported vs. NHE.

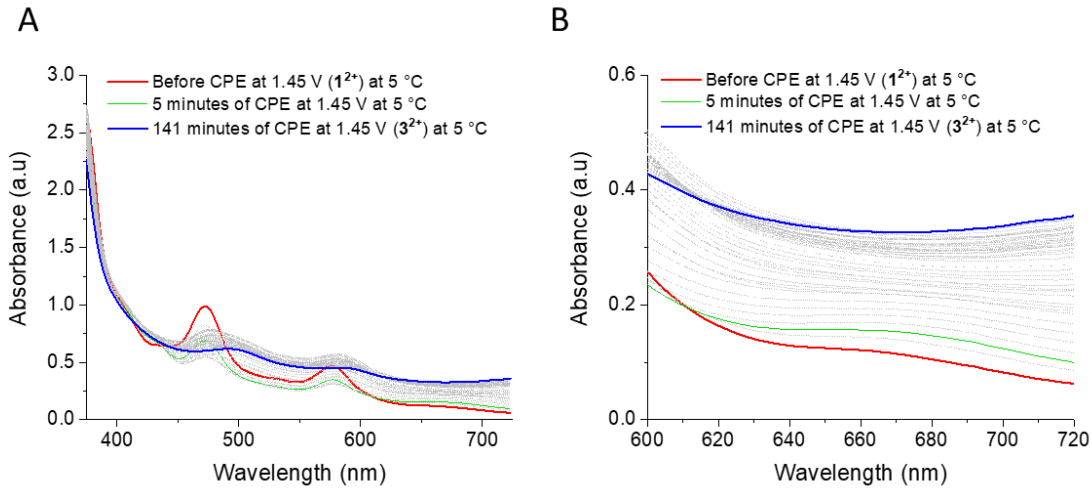

Figure S23. Spectral changes recorded with UV-Vis probe before (red) and after (blue) a CPE at E_{app}= 1.45 V in a phosphate buffer solution at pH 9 (T= 5 ℃). Conditions: 50 ml of buffered solution (sodium borate buffer, pH 9) of $\mathbf{1}^{2+}$ ([$\mathbf{1}^{2+}$] = 0.2 mM, 10 μmol). WE: Pt net electrode (simple cylindrical Pt wire electrode, diameter: 35 mm and cylinder height: 50 mm); CE: Pt wire; RE: silver wire, the potential reported vs. NHE.

The equilibrium concentrations of Ru^{III}-O-$^{III}Ru^{4+}$, $[Ru^{III}$-O-$^{III}Ru^{4+}]_e$, were calculated from the spectral changes after adding various concentrations of oxidant ($NaIO_4$) and the known dimer extinction coefficient at λ = 791 nm (7281.6 $M^{-1}\cdot mm^{-1}$). In order to calculate $[Ru^{III}$-$OH^{2+}]_e$, first the starting concentration of Ru^{III}-OH^{2+}, $[Ru^{III}$-$OH^{2+}]_o$, was calculated from spectral changes of [$\mathbf{1}^{2+}$] after adding various amounts of oxidant and the known extinction coefficient of $\mathbf{1}^{2+}$ at λ = 472 nm (ε = 6472.52 $M^{-1}\cdot mm^{-1}$). Then, $[Ru^{III}$-$OH^{2+}]_e$ was calculated from Eq S1 (Table S4).

$$[Ru^{III}\text{-}OH^{2+}]_e = [Ru^{III}\text{-}OH^{2+}]_o - 2\,[Ru^{III}\text{-}O\text{-}^{III}Ru^{4+}]_e \qquad \text{(Eq. S1)}$$

Table S4. Absorbance changes for after addition of various concentrations of oxidant $NaIO_4$ to $\mathbf{1}^{2+}$.

$\mathbf{1}^{2+}$:$NaIO_4$	A (471 nm) ($\mathbf{1}^{2+}$)	ΔA (at 471 nm) ($\mathbf{2}^{2+}$)	ΔA (at 791 nm) ($\mathbf{3}^{4+}$)
1-0.5	0.616	0.570	0.02032
1-1	0.621	0.4883	0.0405
1-2	0.605	0.3081	0.12150
1-3	0.564	0.1852	0.12239

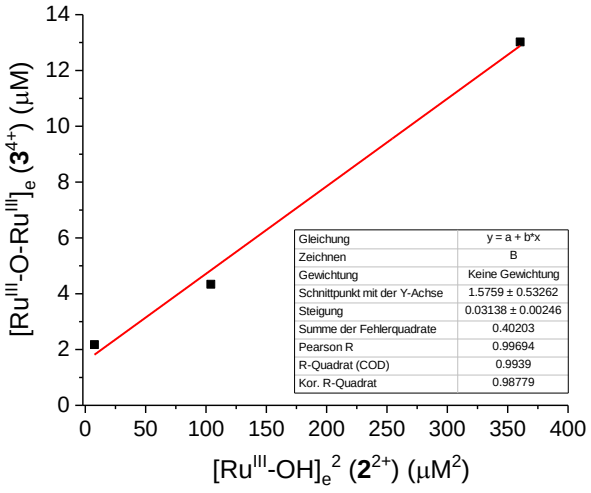

Figure S24. Linear plot of $[Ru^{III}$-O-$^{III}Ru^{4+}]_e$ ($[\mathbf{3}^{4+}]_e$) vs. $[Ru^{III}$-$OH^{2+}]_e^2$, ($[\mathbf{2}^{2+}]_e^2$) to estimate the value of equilibrium constant K_e for the dimerization reaction.

Electrochemistry in organic and aqueous solutions

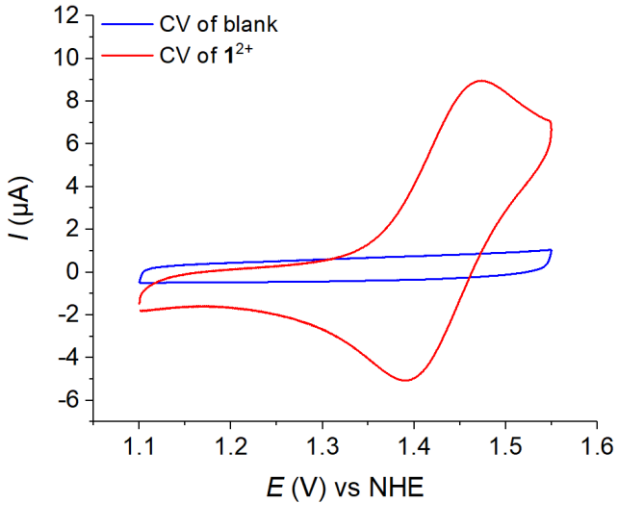

Figure S25. CV of $\mathbf{1}^{2+}$ (1 mM) in a solution of TFE and 0.1 M $(Bu_4N)PF_6$ at scan rate of 100 mV/s WE: glassy carbon electrode; CE: platinum electrode; RE: Hg/Hg_2SO_4.

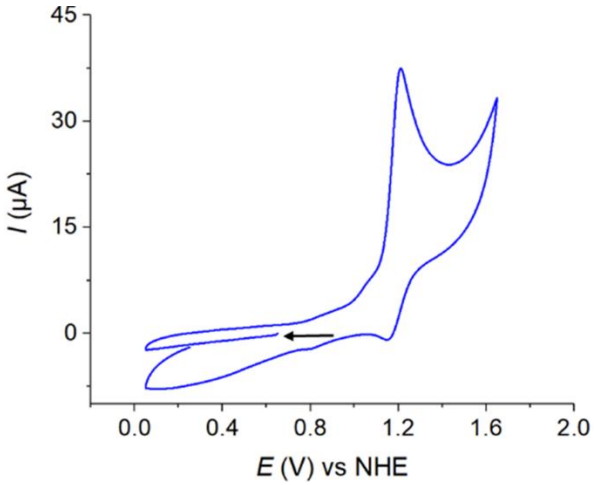

Figure S26. CV of $\mathbf{1}^{2+}$ in a phbf aqueous solution at pH 7 in cathodic direction. Conditions: [$\mathbf{1}^{2+}$]: 1mM, scan rate: 100 mV/s. WE: glassy carbon electrode; CE: platinum electrode; RE: Hg/Hg_2SO_4. Black arrows show the scan direction.

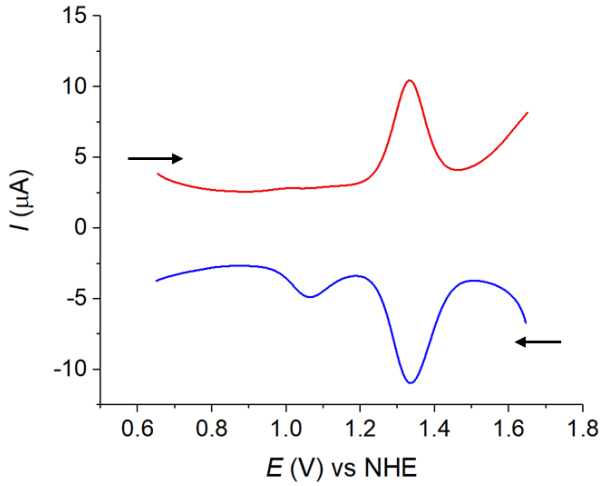

Figure S27. DPV of $\mathbf{1}^{2+}$ in anodic (red line) and cathodic (blue line) directions. WE: glassy carbon electrode; CE: platinum electrode; RE: Hg/Hg_2SO_4. Black arrows show the scan direction.

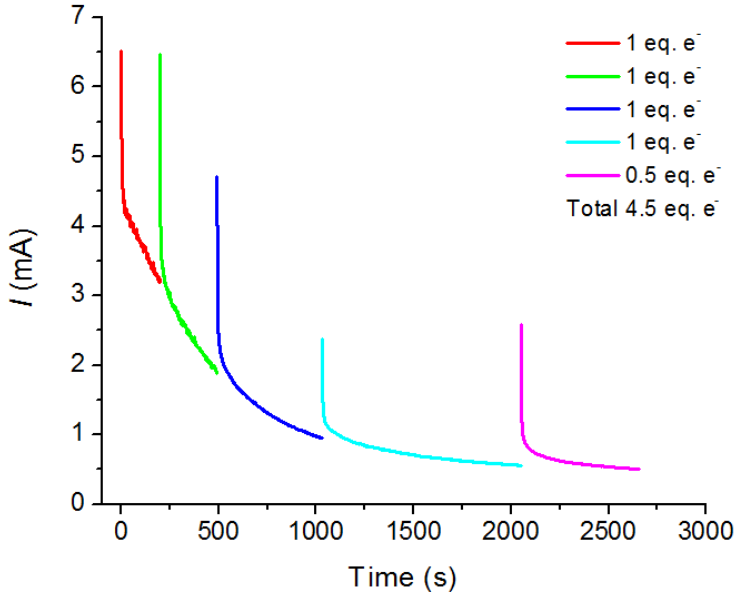

Figure S28. CPE at E_{app} = 1.45 V vs. NHE of a solution of $\mathbf{1}^{2+}$ (1.34 mM, 5 mL, pD 7 phbf; 6.7 μmols) using a Pt net electrode (simple cylindrical Pt net electrode, diameter: 10 mm and cylinder height: 30 mm) as a working electrode, Hg/Hg_2SO_4 as reference electrode and a Pt mesh as auxiliary electrode (simple square mesh net 20*20 mm). The charge passed was integrated to be 3.37 C, giving 5 equivalents of electrons.

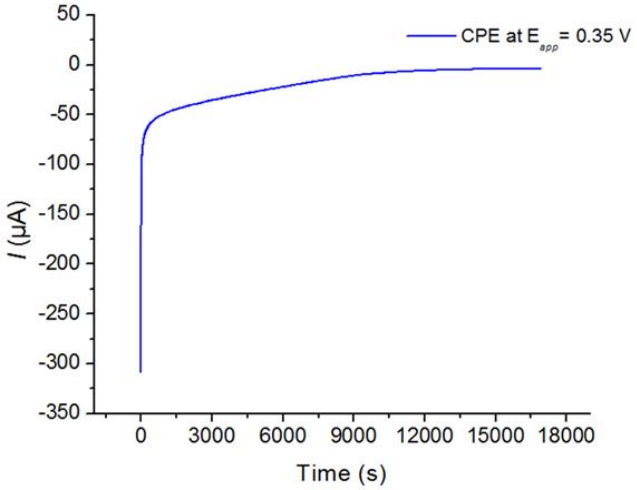

Figure S29. CPE at E_{app} = 0.35 V vs. NHE of a solution of $\mathbf{3}^{4+}$ (0.67 mM, 2 mL, pD 7 phbf; 1.34 µmols) using a Pt net electrode (simple cylindrical Pt net electrode, diameter: 10 mm and cylinder height: 30 mm) as a working electrode, Hg/Hg_2SO_4 as reference electrode and a Pt mesh as auxiliary electrode (simple square mesh net 20*20 mm). The charge passed was integrated to be 0.32 C, giving 2.5 equivalents of electrons.

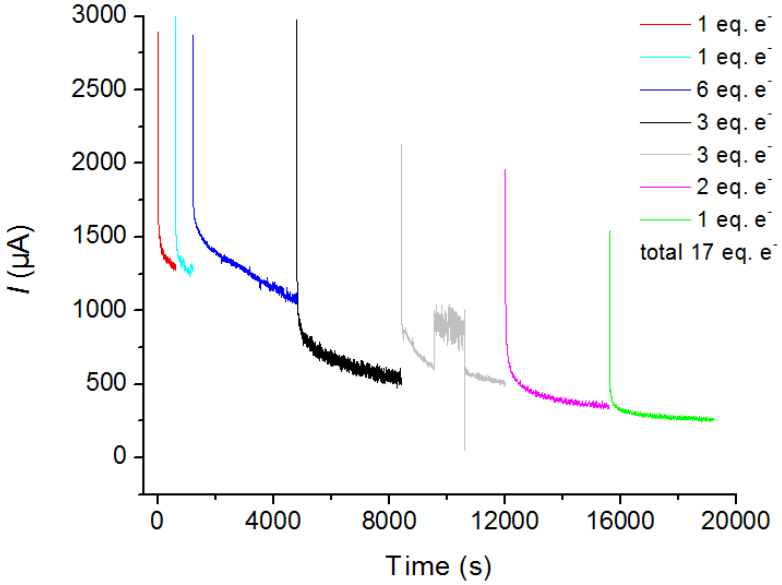

Figure S30. CPE at E_{app}= 1.65 V vs. NHE of a solution of $\mathbf{1}^{2+}$ (1 mM, 6 mL, pH 1 (TA:TFE/2:1); 8.04 µmols) using a Pt net electrode (simple cylindrical Pt net electrode, diameter: 10 mm and cylinder height: 30 mm) as a working electrode, Hg/Hg_2SO_4 as reference electrode and a Pt mesh as auxiliary electrode (simple square mesh net 20*20 mm). The charge passed was integrated to be 13.52 C, giving 16.8 equivalents of electrons.

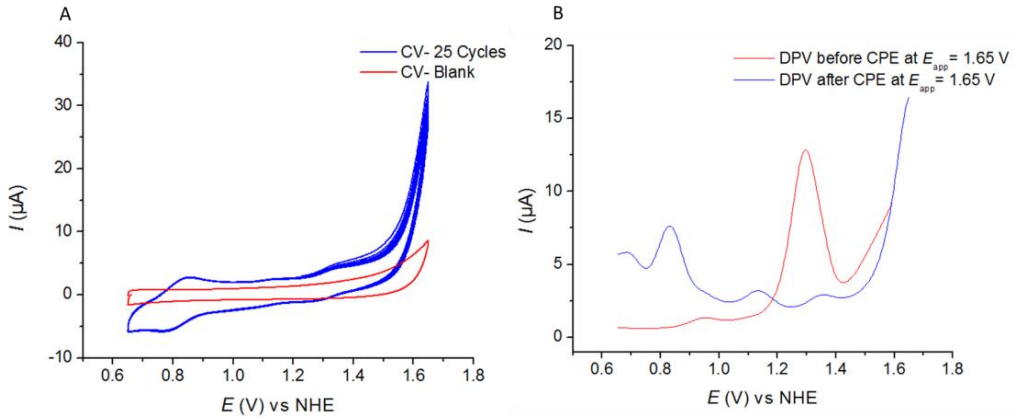

Figure S31. A) 25 Consecutive CVs after CPE at E_{app}= 1.65 V (Figure S30) in a solution of $\mathbf{1}^{2+}$ at pH 1 (TA:TFE (2:1), [TA]= 0.1 M) at scan rate 100 mV/s that generates complex $\mathbf{4}^{2+}$. B) DPV of $\mathbf{1}^{2+}$ (1 mM) before and after CPE. WE: glassy carbon electrode; CE: platinum electrode; RE: Hg/Hg_2SO_4. Black arrows show the scan direction.

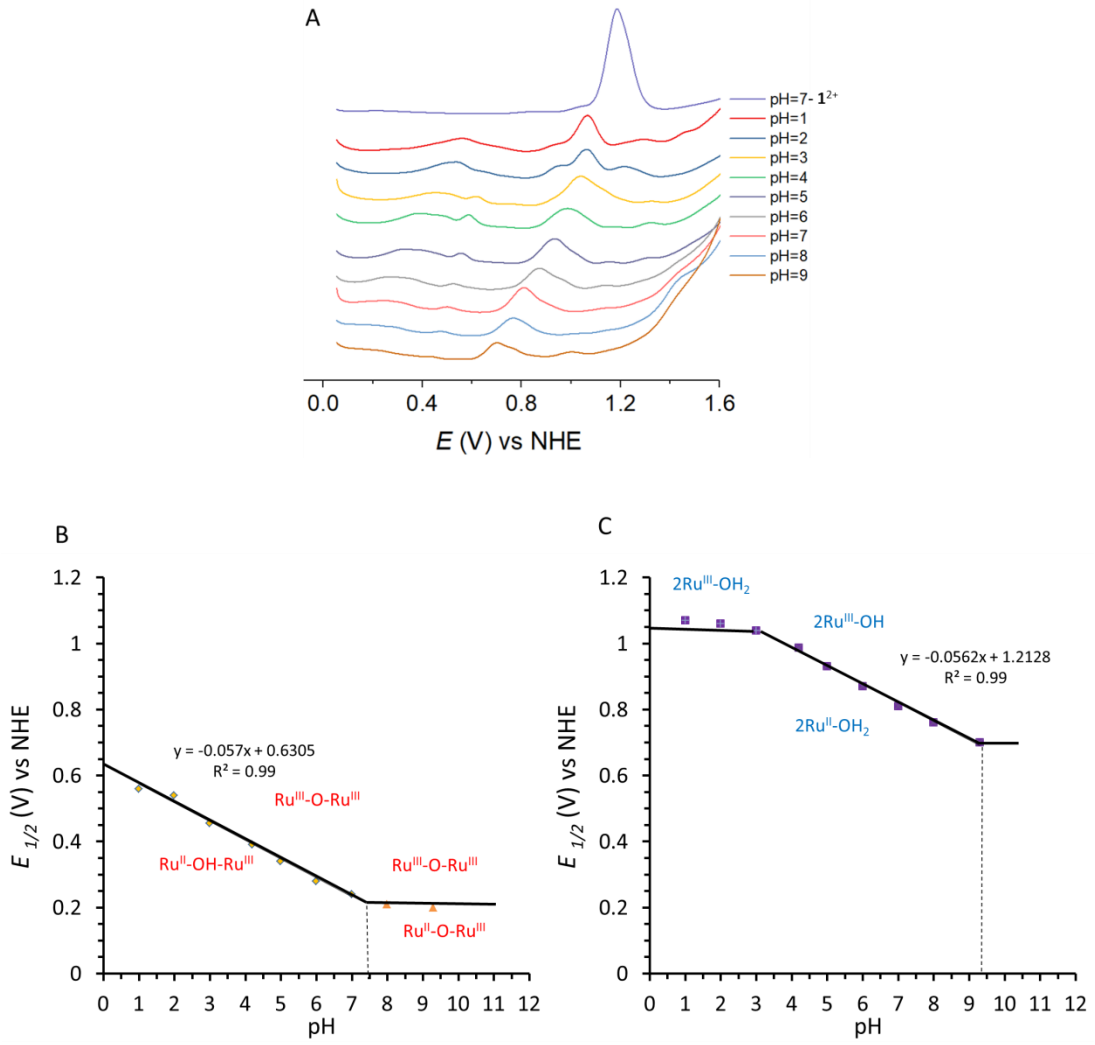

Figure S32. A) DPV of $\mathbf{1}^{2+}$ before CPE at pH 7 (light purple) and DPVs after CPE at E_{app}= 1.45 V at different pH values (pH 1-9), the pH of CPE solution was changed from 7 to 1 and from 7 to 12 gradually by adding phosphoric acid and concentrated NaOH, respectively. DPV was measured at each different pH and the redox waves were taken from DPVs. B) Pourbaix diagram for $\mathbf{3}^{4+}$ after CPE at E_{app}= 1.45 V in a phbf aqueous solution at pH 7, C) Pourbaix diagram for $\mathbf{4}^{2+}$ after CPE at E_{app}= 1.45 V in a phosphate buffer solution at pH 7.

Crystallographic data

Table S5. Crystal data and structure refinement for **1**Cl_2.

Identification code	mo_Abi3903b_0m	
Empirical formula	C76 H64 Cl12 N12 Ru2	
Formula weight	1772.93	
Temperature	100(2)K	
Wavelength	0.71073 Å	
Crystal system	monoclinic	
Space group	$P2_1$	
Unit cell dimensions	a = 10.6462(13)Å	a= 90°.
	b = 9.5942(13)Å	b = 98.317(5)°.
	c = 17.992(2)Å	γ = 90°.
Volume	1818.4(4) $Å^3$	
Z	1	
Density (calculated)	1.619 Mg/m^3	
Absorption coefficient	0.911 mm^{-1}	
F(000)	896	
Crystal size	0.150 x 0.100 x 0.050 mm^3	
Theta range for data collection	1.144 to 25.426°.	
Index ranges	-12 ≤ h ≤ 12,-9 ≤ k ≤ 11,-21 ≤ l ≤ 21	
Reflections collected	14827	
Independent reflections	6104[R(int) = 0.0681]	
Completeness to theta =25.426°	99.1%	
Absorption correction	Multi-scan	
Max. and min. transmission	0.74 and 0.55	
Refinement method	Full-matrix least-squares on F^2	
Data / restraints / parameters	6104/ 49/ 463	
Goodness-of-fit on F^2	1.032	
Final R indices [I>2sigma(I)]	R1 = 0.0544, wR2 = 0.1095	
R indices (all data)	R1 = 0.0732, wR2 = 0.1172	
Largest diff. peak and hole	1.148 and -0.566 e.$Å^{-3}$	

Table S6. Bond lengths [Å] and angles [°] for **1**Cl_2.

Bond lengths----

Ru1	N2	1.942(7)	C2	C3	1.359(14)	C19	C22	1.400(13)
Ru1	N3	1.960(7)	C3	C4	1.417(14)	C19	C20	1.424(12)
Ru1	N6	2.088(7)	C4	C5	1.405(12)	C20	C21	1.346(14)
Ru1	N5	2.088(7)	C4	C9	1.426(13)	C22	C23	1.372(14)
Ru1	N4	2.188(8)	C5	C6	1.411(15)	C23	C24	1.404(13)
Ru1	N1	2.202(8)	C6	C7	1.409(13)	C25	C26	1.367(12)
N1	C1	1.319(12)	C7	C10	1.394(14)	C26	C27	1.389(13)
N1	C5	1.380(12)	C7	C8	1.431(14)	C27	C28	1.384(14)
N2	C12	1.354(12)	C8	C9	1.346(14)	C27	C30	1.511(12)
N2	C6	1.361(12)	C10	C11	1.394(13)	C28	C29	1.378(12)
N3	C17	1.334(11)	C11	C12	1.404(13)	C31	C32	1.377(13)
N3	C13	1.335(11)	C12	C13	1.475(13)	C32	C33	1.404(14)
N4	C24	1.313(11)	C13	C14	1.407(13)	C33	C34	1.371(13)
N4	C18	1.387(12)	C14	C15	1.384(13)	C33	C36	1.522(13)
N5	C25	1.337(11)	C15	C16	1.409(13)	C34	C35	1.379(13)
N5	C29	1.346(11)	C16	C17	1.396(12)	C1S	Cl1S	1.766(11)
N6	C35	1.339(11)	C16	C21	1.435(13)	C1S	Cl2S	1.780(11)
N6	C31	1.344(12)	C17	C18	1.436(14)	C2S	Cl4S	1.773(12)
C1	C2	1.413(13)	C18	C19	1.406(12)	C2S	Cl3S	1.774(11)

Angles----------

N6	Ru1	N1	87.8(3)	N1	C5	C4	123.5(10)	N4	C18	C19	124.7(10)
N5	Ru1	N1	88.7(3)	N1	C5	C6	118.7(8)	N4	C18	C17	117.5(7)
N4	Ru1	N1	122.5(3)	C4	C5	C6	117.8(9)	C19	C18	C17	117.8(9)
C1	N1	C5	117.8(8)	N2	C6	C7	120.8(9)	C22	C19	C18	116.6(9)
C1	N1	Ru1	134.6(7)	N2	C6	C5	115.5(9)	C22	C19	C20	124.8(9)
C5	N1	Ru1	107.5(6)	C7	C6	C5	123.8(9)	C18	C19	C20	118.5(9)
C12	N2	C6	121.9(8)	C10	C7	C6	117.6(9)	C21	C20	C19	123.6(9)
C12	N2	Ru1	119.4(6)	C10	C7	C8	126.3(9)	C20	C21	C16	119.5(9)
C6	N2	Ru1	118.7(7)	C6	C7	C8	116.1(10)	C23	C22	C19	118.6(9)
C17	N3	C13	122.4(8)	C9	C8	C7	121.2(10)	C22	C23	C24	121.1(9)
C17	N3	Ru1	118.7(6)	C8	C9	C4	122.4(10)	N4	C24	C23	122.8(9)
C13	N3	Ru1	118.9(6)	C11	C10	C7	121.0(10)	N5	C25	C26	124.6(9)
C24	N4	C18	116.2(8)	C10	C11	C12	119.2(10)	C25	C26	C27	119.1(9)

C24	N4	Ru1	135.5(6)	N2	C12	C11	119.5(9)	C28	C27	C26	117.2(8)
C18	N4	Ru1	108.3(6)	N2	C12	C13	111.0(8)	C28	C27	C30	122.2(9)
C25	N5	C29	116.0(8)	C11	C12	C13	129.4(9)	C26	C27	C30	120.5(9)
C25	N5	Ru1	119.7(6)	N3	C13	C14	119.6(8)	C29	C28	C27	119.8(9)
C29	N5	Ru1	124.3(6)	N3	C13	C12	112.2(8)	N5	C29	C28	123.2(9)
C35	N6	C31	116.6(8)	C14	C13	C12	128.1(9)	N6	C31	C32	124.0(9)
C35	N6	Ru1	118.6(6)	C15	C14	C13	118.7(9)	C31	C32	C33	118.5(9)
C31	N6	Ru1	124.8(6)	C14	C15	C16	121.0(9)	C34	C33	C32	117.4(8)
N1	C1	C2	122.5(10)	C17	C16	C15	116.6(9)	C34	C33	C36	121.7(8)
C3	C2	C1	119.9(10)	C17	C16	C21	118.2(9)	C32	C33	C36	120.9(9)
C2	C3	C4	119.9(9)	C15	C16	C21	125.2(9)	C33	C34	C35	120.3(8)
C5	C4	C3	116.4(10)	N3	C17	C16	121.7(9)	N6	C35	C34	123.0(9)
C5	C4	C9	118.8(10)	N3	C17	C18	115.9(8)	Cl1S	C1S	Cl2S	109.7(6)
C3	C4	C9	124.8(9)	C16	C17	C18	122.4(8)	Cl4S	C2S	Cl3S	110.2(5)

Table S7. Torsion angles [°] for **1**Cl_2.

C5	N1	C1	C2	0.9(13)	C14	C15	C16	C21	179.9(8)
Ru1	N1	C1	C2	-176.2(7)	C13	N3	C17	C16	1.4(13)
N1	C1	C2	C3	-1.9(14)	Ru1	N3	C17	C16	178.8(6)
C1	C2	C3	C4	1.4(14)	C13	N3	C17	C18	179.0(7)
C2	C3	C4	C5	0.0(13)	Ru1	N3	C17	C18	-3.6(10)
C2	C3	C4	C9	-179.2(9)	C15	C16	C17	N3	-0.2(13)
C1	N1	C5	C4	0.7(12)	C21	C16	C17	N3	179.0(8)
Ru1	N1	C5	C4	178.5(7)	C15	C16	C17	C18	-177.6(8)
C1	N1	C5	C6	178.9(8)	C21	C16	C17	C18	1.6(13)
Ru1	N1	C5	C6	-3.3(9)	C24	N4	C18	C19	0.7(12)
C3	C4	C5	N1	-1.1(12)	Ru1	N4	C18	C19	-178.4(6)
C9	C4	C5	N1	178.2(8)	C24	N4	C18	C17	-179.2(7)
C3	C4	C5	C6	-179.3(8)	Ru1	N4	C18	C17	1.7(8)
C9	C4	C5	C6	0.0(12)	N3	C17	C18	N4	0.9(11)
C12	N2	C6	C7	0.2(13)	C16	C17	C18	N4	178.5(8)
Ru1	N2	C6	C7	-178.2(7)	N3	C17	C18	C19	-178.9(7)
C12	N2	C6	C5	179.8(8)	C16	C17	C18	C19	-1.4(12)
Ru1	N2	C6	C5	1.4(10)	N4	C18	C19	C22	-1.1(12)
N1	C5	C6	N2	1.6(12)	C17	C18	C19	C22	178.8(7)
C4	C5	C6	N2	179.9(7)	N4	C18	C19	C20	-179.9(7)
N1	C5	C6	C7	-178.7(8)	C17	C18	C19	C20	0.0(11)
C4	C5	C6	C7	-0.4(13)	C22	C19	C20	C21	-177.5(9)

N2	C6	C7	C10	-1.4(13)	C18	C19	C20	C21	1.1(13)
C5	C6	C7	C10	179.0(8)	C19	C20	C21	C16	-0.9(14)
N2	C6	C7	C8	179.6(8)	C17	C16	C21	C20	-0.4(13)
C5	C6	C7	C8	0.0(14)	C15	C16	C21	C20	178.7(9)
C10	C7	C8	C9	-177.9(9)	C18	C19	C22	C23	1.6(12)
C6	C7	C8	C9	1.0(14)	C20	C19	C22	C23	-179.7(8)
C7	C8	C9	C4	-1.5(15)	C19	C22	C23	C24	-1.9(13)
C5	C4	C9	C8	1.0(14)	C18	N4	C24	C23	-0.9(12)
C3	C4	C9	C8	-179.8(10)	Ru1	N4	C24	C23	177.9(6)
C6	C7	C10	C11	2.1(14)	C22	C23	C24	N4	1.6(14)
C8	C7	C10	C11	-179.0(9)	C29	N5	C25	C26	0.4(13)
C7	C10	C11	C12	-1.7(13)	Ru1	N5	C25	C26	-178.8(7)
C6	N2	C12	C11	0.4(12)	N5	C25	C26	C27	-0.6(14)
Ru1	N2	C12	C11	178.7(6)	C25	C26	C27	C28	0.7(13)
C6	N2	C12	C13	-177.2(7)	C25	C26	C27	C30	178.8(8)
Ru1	N2	C12	C13	1.2(9)	C26	C27	C28	C29	-0.7(13)
C10	C11	C12	N2	0.4(12)	C30	C27	C28	C29	-178.7(9)
C10	C11	C12	C13	177.5(9)	C25	N5	C29	C28	-0.4(13)
C17	N3	C13	C14	-1.4(13)	Ru1	N5	C29	C28	178.8(7)
Ru1	N3	C13	C14	-178.8(6)	C27	C28	C29	N5	0.6(14)
C17	N3	C13	C12	176.1(7)	C35	N6	C31	C32	1.5(13)
Ru1	N3	C13	C12	-1.2(10)	Ru1	N6	C31	C32	-178.2(7)
N2	C12	C13	N3	0.1(10)	N6	C31	C32	C33	-3.5(15)
C11	C12	C13	N3	-177.2(8)	C31	C32	C33	C34	3.0(14)
N2	C12	C13	C14	177.4(8)	C31	C32	C33	C36	-178.5(9)
C11	C12	C13	C14	0.1(15)	C32	C33	C34	C35	-0.9(14)
N3	C13	C14	C15	0.2(12)	C36	C33	C34	C35	-179.4(9)
C12	C13	C14	C15	-176.9(8)	C31	N6	C35	C34	0.8(13)
C13	C14	C15	C16	1.0(13)	Ru1	N6	C35	C34	-179.5(7)
C14	C15	C16	C17	-1.0(13)	C33	C34	C35	N6	-1.1(15)

Symmetry operations: 1 'x, y, z'; 2 '-x, y+1/2, -z'

Table S8. Crystal data and structure refinement for **4**$(CF_3SO_3)_2$.

Identification code	mo_Abi914_0m	
Empirical formula	C33.60 H27.80 F6 N5 O7.80 Ru S2	
Formula weight	905.60	
Temperature	100(2)K	
Wavelength	0.71073 Å	
Crystal system	monoclinic	
Space group	*C*2/c	
Unit cell dimensions	a = 23.8599(17)Å	a= 90°.
	b = 13.0679(9)Å	b = 93.5948(19)°.
	c = 26.5063(18)Å	γ = 90°.
Volume	8248.4(10) $Å^3$	
Z	8	
Density (calculated)	1.458 Mg/m^3	
Absorption coefficient	0.559 mm^{-1}	
F(000)	3654	
Crystal size	0.100 x 0.050 x 0.010 mm^3	
Theta range for data collection	1.710 to 27.922°.	
Index ranges	-31 ≤ h ≤ 31,-17 ≤ k ≤ 14,-34 ≤ l ≤ 33	
Reflections collected	64035	
Independent reflections	9835[R(int) = 0.0570]	
Completeness to theta =27.922°	99.6%	
Absorption correction	Multi-scan	
Max. and min. transmission	0.74 and 0.46	
Refinement method	Full-matrix least-squares on F^2	
Data / restraints / parameters	9835/ 2080/ 912	
Goodness-of-fit on F^2	1.082	
Final R indices [I>2sigma(I)]	R1 = 0.0735, wR2 = 0.2088	
R indices (all data)	R1 = 0.0962, wR2 = 0.2302	
Largest diff. peak and hole	1.345 and -0.784 e.$Å^{-3}$	

Table S9. Bond lengths [Å] and angles [°] for **4**$(CF_3SO_3)_2$.

Bond lengths----

Ru1	N2'	1.927(7)	C8'	C10'	1.444(9)	C1B	F1B	1.311(8)
Ru1	N3	1.936(4)	C10'	C11'	1.346(10)	C1B	F2B	1.319(8)
Ru1	N2	1.980(15)	C11'	C12'	1.420(8)	C1B	F3B	1.330(8)
Ru1	N5	2.061(4)	C12'	C13	1.493(10)	S1B'	O3B'	1.440(10)
Ru1	O1	2.104(4)	N3	C13	1.352(7)	S1B'	O2B'	1.450(10)
Ru1	N4	2.168(4)	N3	C17	1.357(7)	S1B'	O1B'	1.455(10)
Ru1	N1'	2.173(7)	N4	C24	1.322(7)	S1B'	C1B'	1.828(10)
Ru1	N1	2.179(15)	N4	C21	1.374(7)	O1B'	O3B'	1.66(4)
N1	C1	1.346(10)	C13	C14	1.420(8)	C1B'	F3B'	1.311(10)
N1	C4	1.382(9)	C14	C15	1.384(10)	C1B'	F2B'	1.319(10)
N2	C9	1.350(9)	C15	C16	1.384(10)	C1B'	F1B'	1.326(10)
N2	C12	1.355(10)	C16	C17	1.391(8)	S1A	O2A	1.413(9)
C1	C2	1.433(11)	C16	C18	1.422(9)	S1A	O3A	1.420(9)
C2	C3	1.344(12)	C17	C21	1.428(8)	S1A	O1A	1.433(9)
C3	C5	1.429(10)	C18	C19	1.351(10)	S1A	C1A	1.812(10)
C4	C5	13.900	C19	C20	1.454(9)	O2A	C1A	1.82(2)
C4	C9	13.900	C20	C22	1.396(9)	C1A	F1A	1.304(9)
C5	C6	13.900	C20	C21	1.403(7)	C1A	F2A	1.310(9)
C6	C7	13.900	C22	C23	1.335(9)	C1A	F3A	1.323(10)
C7	C8	13.900	C23	C24	1.422(7)	S1A'	O3A'	1.450(6)
C8	C9	13.900	N5	C29'	1.23(4)	S1A'	O2A'	1.459(7)
C8	C10	1.452(10)	N5	C25'	1.34(3)	S1A'	O1A'	1.479(7)
C10	C11	1.341(11)	N5	C25	1.350(14)	S1A'	C1A'	1.837(9)
C11	C12	1.420(10)	N5	C29	1.373(19)	C1A'	F3A'	1.325(8)
C12	C13	1.423(17)	C25	C26	1.402(17)	C1A'	F1A'	1.333(8)
N1'	C1'	1.347(8)	C26	C27	1.368(14)	C1A'	F2A'	1.354(9)
N1'	C4'	1.375(7)	C27	C28	1.347(17)	O1S	C1S	1.432(10)
N2'	C9'	1.352(7)	C27	C30	1.524(16)	O1S	C3S	1.438(10)
N2'	C12'	1.354(8)	C28	C29	1.355(19)	C1S	C2S	1.539(10)
C1'	C2'	1.430(9)	C25'	C26'	1.36(3)	C3S	C4S	1.541(10)
C2'	C3'	1.347(10)	C26'	C27'	1.38(3)	O1S'	C1S'	1.424(10)
C3'	C5'	1.422(9)	C27'	C28'	1.35(3)	O1S'	C3S'	1.427(10)
C4'	C5'	1.392(7)	C27'	C30'	1.57(3)	C1S'	C2S'	1.541(10)

C4'	C9'	1.407(7)	C28'	C29'	1.44(4)	C1S'	C3S'	1.92(6)
C5'	C6'	1.421(7)	S1B	O1B	1.399(4)	C3S'	C4S'	1.539(10)
C6'	C7'	1.375(8)	S1B	O3B	1.421(5)	O1W	O1W#	1.79(6) 2_656
C7'	C8'	1.408(7)	S1B	O2B	1.460(5)	O1W"	O1W"#	1.28(10) 2_656
C8'	C9'	1.397(7)	S1B	C1B	1.792(7)			

Angles----------

N2'	Ru1	N3	79.9(2)	C4'	C5'	C3'	117.0(6)	O1B	S1B	O3B	118.1(4)
N3	Ru1	N2	77.0(4)	C6'	C5'	C3'	124.3(6)	O1B	S1B	O2B	115.7(3)
N2'	Ru1	N5	96.0(3)	C7'	C6'	C5'	122.2(6)	O3B	S1B	O2B	113.2(4)
N3	Ru1	N5	91.70(17)	C6'	C7'	C8'	119.7(6)	O1B	S1B	C1B	101.9(4)
N2	Ru1	N5	87.6(7)	C9'	C8'	C7'	117.8(6)	O3B	S1B	C1B	102.7(4)
N2'	Ru1	O1	87.7(3)	C9'	C8'	C10'	116.3(6)	O2B	S1B	C1B	102.0(5)
N3	Ru1	O1	91.47(16)	C7'	C8'	C10'	125.9(6)	F1B	C1B	F2B	110.5(7)
N2	Ru1	O1	96.3(7)	N2'	C9'	C8'	121.6(6)	F1B	C1B	F3B	109.3(7)
N5	Ru1	O1	175.50(15)	N2'	C9'	C4'	115.3(5)	F2B	C1B	F3B	107.7(7)
N2'	Ru1	N4	159.0(2)	C8'	C9'	C4'	123.1(6)	F1B	C1B	S1B	111.3(6)
N3	Ru1	N4	79.42(17)	C11'	C10'	C8'	120.8(6)	F2B	C1B	S1B	108.7(6)
N2	Ru1	N4	155.8(4)	C10'	C11'	C12'	120.6(7)	F3B	C1B	S1B	109.2(6)
N5	Ru1	N4	87.72(16)	N2'	C12'	C11'	118.3(6)	O3B'	S1B'	O2B'	113.9(11)
O1	Ru1	N4	89.72(15)	N2'	C12'	C13	112.0(6)	O3B'	S1B'	O1B'	70.1(18)
N2'	Ru1	N1'	79.1(2)	C11'	C12'	C13	129.5(7)	O2B'	S1B'	O1B'	113.3(10)
N3	Ru1	N1'	158.9(2)	C13	N3	C17	121.6(5)	O3B'	S1B'	C1B'	77.1(16)
N5	Ru1	N1'	91.7(3)	C13	N3	Ru1	119.0(4)	O2B'	S1B'	C1B'	141.4(17)
O1	Ru1	N1'	86.5(3)	C17	N3	Ru1	119.4(3)	O1B'	S1B'	C1B'	105.3(15)
N4	Ru1	N1'	121.5(2)	C24	N4	C21	117.9(4)	S1B'	O1B'	O3B'	54.5(10)
N3	Ru1	N1	154.6(4)	C24	N4	Ru1	133.1(4)	S1B'	O3B'	O1B'	55.4(10)
N2	Ru1	N1	77.8(5)	C21	N4	Ru1	109.0(3)	F3B'	C1B'	F2B'	109.8(11)
N5	Ru1	N1	84.4(6)	N3	C13	C14	118.9(6)	F3B'	C1B'	F1B'	109.5(11)
O1	Ru1	N1	94.1(6)	N3	C13	C12	113.9(8)	F2B'	C1B'	F1B'	107.8(11)
N4	Ru1	N1	125.3(4)	C14	C13	C12	126.3(8)	F3B'	C1B'	S1B'	119(2)
C1	N1	C4	118.7(9)	N3	C13	C12'	110.6(5)	F2B'	C1B'	S1B'	110(2)
C1	N1	Ru1	130.7(9)	C14	C13	C12'	130.5(6)	F1B'	C1B'	S1B'	99.9(19)
C4	N1	Ru1	110.1(7)	C15	C14	C13	118.0(6)	O2A	S1A	O3A	118.4(9)
C9	N2	C12	121.7(9)	C14	C15	C16	123.2(6)	O2A	S1A	O1A	116.0(8)
C9	N2	Ru1	117.6(8)	C15	C16	C17	115.9(5)	O3A	S1A	O1A	125.2(12)

C12	N2	Ru1	119.6(9)	C15	C16	C18	127.7(6)	O2A	S1A	C1A	67.4(10)
N1	C1	C2	120.2(11)	C17	C16	C18	116.3(6)	O3A	S1A	C1A	99.5(13)
C3	C2	C1	120.6(11)	N3	C17	C16	122.3(5)	O1A	S1A	C1A	106.2(12)
C2	C3	C5	120.4(10)	N3	C17	C21	114.2(5)	S1A	O2A	C1A	66.8(7)
N1	C4	C5	123.4(6)	C16	C17	C21	123.4(5)	F1A	C1A	F2A	110.1(10)
N1	C4	C9	116.5(6)	C19	C18	C16	121.9(6)	F1A	C1A	F3A	110.6(10)
C5	C4	C9	120.0	C18	C19	C20	122.3(6)	F2A	C1A	F3A	109.6(10)
C4	C5	C6	120.0	C22	C20	C21	117.3(6)	F1A	C1A	S1A	110.2(12)
C4	C5	C3	116.5(7)	C22	C20	C19	125.9(5)	F2A	C1A	S1A	111.7(12)
C6	C5	C3	123.5(7)	C21	C20	C19	116.8(6)	F3A	C1A	S1A	104.5(14)
C7	C6	C5	120.0	N4	C21	C20	122.9(5)	F1A	C1A	O2A	79.7(10)
C8	C7	C6	120.0	N4	C21	C17	117.9(4)	F2A	C1A	O2A	92.6(11)
C9	C8	C7	120.0	C20	C21	C17	119.2(5)	F3A	C1A	O2A	149.1(14)
C9	C8	C10	115.1(7)	C23	C22	C20	119.9(5)	S1A	C1A	O2A	45.8(4)
C7	C8	C10	124.8(7)	C22	C23	C24	120.5(6)	O3A'	S1A'	O2A'	109.4(6)
N2	C9	C8	122.9(6)	N4	C24	C23	121.4(5)	O3A'	S1A'	O1A'	111.4(6)
N2	C9	C4	116.7(6)	C29'	N5	C25'	123(2)	O2A'	S1A'	O1A'	109.0(6)
C8	C9	C4	120.0	C25	N5	C29	114.4(11)	O3A'	S1A'	C1A'	99.5(7)
C11	C10	C8	121.0(10)	C29'	N5	Ru1	118.6(15)	O2A'	S1A'	C1A'	127.5(7)
C10	C11	C12	121.1(11)	C25'	N5	Ru1	117.6(12)	O1A'	S1A'	C1A'	99.4(6)
N2	C12	C11	117.9(10)	C25	N5	Ru1	117.8(7)	F3A'	C1A'	F1A'	106.2(8)
N2	C12	C13	110.1(11)	C29	N5	Ru1	127.1(8)	F3A'	C1A'	F2A'	108.8(8)
C11	C12	C13	131.7(11)	N5	C25	C26	122.7(11)	F1A'	C1A'	F2A'	106.6(8)
C1'	N1'	C4'	117.5(6)	C27	C26	C25	119.9(10)	F3A'	C1A'	S1A'	112.1(7)
C1'	N1'	Ru1	133.7(5)	C28	C27	C26	118.1(11)	F1A'	C1A'	S1A'	112.5(7)
C4'	N1'	Ru1	108.9(4)	C28	C27	C30	121.4(11)	F2A'	C1A'	S1A'	110.4(8)
C9'	N2'	C12'	122.4(6)	C26	C27	C30	120.3(10)	C1S	O1S	C3S	126(4)
C9'	N2'	Ru1	119.2(4)	C27	C28	C29	120.2(14)	O1S	C1S	C2S	119.0(18)
C12'	N2'	Ru1	118.4(5)	C28	C29	N5	124.6(17)	O1S	C3S	C4S	117.6(17)
N1'	C1'	C2'	120.9(7)	N5	C25'	C26'	121(2)	C1S'	O1S'	C3S'	85(3)
C3'	C2'	C1'	121.0(7)	C25'	C26'	C27'	117.7(18)	O1S'	C1S'	C2S'	120.8(18)
C2'	C3'	C5'	119.3(6)	C28'	C27'	C26'	119.9(19)	O1S'	C1S'	C3S'	47.7(16)
N1'	C4'	C5'	124.3(5)	C28'	C27'	C30'	118.5(19)	C2S'	C1S'	C3S'	168(3)
N1'	C4'	C9'	117.4(5)	C26'	C27'	C30'	121.5(17)	O1S'	C3S'	C4S'	119.7(18)
C5'	C4'	C9'	118.3(5)	C27'	C28'	C29'	118(3)	O1S'	C3S'	C1S'	47.6(16)
C4'	C5'	C6'	118.7(6)	N5	C29'	C28'	120(3)	C4S'	C3S'	C1S'	153(5)

Table S10. Torsion angles [°] for **4**$(CF_3SO_3)_2$.

C4	N1	C1	C2	5(3)	Ru1	N3	C17	C16	177.1(4)
Ru1	N1	C1	C2	175.7(17)	C13	N3	C17	C21	179.4(5)
N1	C1	C2	C3	-2(3)	Ru1	N3	C17	C21	-2.9(6)
C1	C2	C3	C5	0(3)	C15	C16	C17	N3	0.3(9)
C1	N1	C4	C5	-7(3)	C18	C16	C17	N3	-178.8(6)
Ru1	N1	C4	C5	-178.9(9)	C15	C16	C17	C21	-179.8(6)
C1	N1	C4	C9	176.8(17)	C18	C16	C17	C21	1.2(9)
Ru1	N1	C4	C9	4.5(17)	C15	C16	C18	C19	179.9(7)
N1	C4	C5	C6	-176.5(17)	C17	C16	C18	C19	-1.2(10)
C9	C4	C5	C6	0.0	C16	C18	C19	C20	0.0(11)
N1	C4	C5	C3	4.3(19)	C18	C19	C20	C22	-179.2(7)
C9	C4	C5	C3	-179.2(15)	C18	C19	C20	C21	1.2(9)
C2	C3	C5	C4	-1(2)	C24	N4	C21	C20	0.5(8)
C2	C3	C5	C6	180.0(16)	Ru1	N4	C21	C20	-177.6(4)
C4	C5	C6	C7	0.0	C24	N4	C21	C17	-179.8(5)
C3	C5	C6	C7	179.2(17)	Ru1	N4	C21	C17	2.1(6)
C5	C6	C7	C8	0.0	C22	C20	C21	N4	-1.1(8)
C6	C7	C8	C9	0.0	C19	C20	C21	N4	178.6(5)
C6	C7	C8	C10	176.6(18)	C22	C20	C21	C17	179.2(5)
C12	N2	C9	C8	8(3)	C19	C20	C21	C17	-1.1(8)
Ru1	N2	C9	C8	175.9(9)	N3	C17	C21	N4	0.2(7)
C12	N2	C9	C4	-179.5(18)	C16	C17	C21	N4	-179.8(5)
Ru1	N2	C9	C4	-11(2)	N3	C17	C21	C20	179.9(5)
C7	C8	C9	N2	172.5(19)	C16	C17	C21	C20	0.0(9)
C10	C8	C9	N2	-4.4(19)	C21	C20	C22	C23	-0.7(9)
C7	C8	C9	C4	0.0	C19	C20	C22	C23	179.6(6)
C10	C8	C9	C4	-176.9(16)	C20	C22	C23	C24	3.0(10)
N1	C4	C9	N2	3.7(18)	C21	N4	C24	C23	1.9(8)
C5	C4	C9	N2	-173.0(18)	Ru1	N4	C24	C23	179.4(4)
N1	C4	C9	C8	176.7(16)	C22	C23	C24	N4	-3.7(9)
C5	C4	C9	C8	0.0	C29	N5	C25	C26	0.1(16)
C9	C8	C10	C11	-1(3)	Ru1	N5	C25	C26	-171.4(8)
C7	C8	C10	C11	-177.7(17)	N5	C25	C26	C27	0.0(16)
C8	C10	C11	C12	3(3)	C25	C26	C27	C28	0.3(17)
C9	N2	C12	C11	-5(3)	C25	C26	C27	C30	176.0(11)

Ru1	N2	C12	C11	-173.3(17)	C26	C27	C28	C29	-1(2)
C9	N2	C12	C13	169.3(19)	C30	C27	C28	C29	-176.4(15)
Ru1	N2	C12	C13	1(3)	C27	C28	C29	N5	1(3)
C10	C11	C12	N2	0(3)	C25	N5	C29	C28	-1(2)
C10	C11	C12	C13	-173(2)	Ru1	N5	C29	C28	170.1(13)
C4'	N1'	C1'	C2'	0.5(13)	C29'	N5	C25'	C26'	6(3)
Ru1	N1'	C1'	C2'	-177.2(7)	Ru1	N5	C25'	C26'	174.2(15)
N1'	C1'	C2'	C3'	0.7(14)	N5	C25'	C26'	C27'	-3(3)
C1'	C2'	C3'	C5'	-1.7(13)	C25'	C26'	C27'	C28'	-1(3)
C1'	N1'	C4'	C5'	-0.6(12)	C25'	C26'	C27'	C30'	-176.1(19)
Ru1	N1'	C4'	C5'	177.5(7)	C26'	C27'	C28'	C29'	1(3)
C1'	N1'	C4'	C9'	179.3(8)	C30'	C27'	C28'	C29'	176(2)
Ru1	N1'	C4'	C9'	-2.5(9)	C25'	N5	C29'	C28'	-6(4)
N1'	C4'	C5'	C6'	177.9(8)	Ru1	N5	C29'	C28'	-174(2)
C9'	C4'	C5'	C6'	-2.1(12)	C27'	C28'	C29'	N5	2(4)
N1'	C4'	C5'	C3'	-0.3(12)	O1B	S1B	C1B	F1B	54.4(7)
C9'	C4'	C5'	C3'	179.7(8)	O3B	S1B	C1B	F1B	-68.3(7)
C2'	C3'	C5'	C4'	1.5(12)	O2B	S1B	C1B	F1B	174.2(6)
C2'	C3'	C5'	C6'	-176.6(8)	O1B	S1B	C1B	F2B	176.4(6)
C4'	C5'	C6'	C7'	0.0(13)	O3B	S1B	C1B	F2B	53.6(7)
C3'	C5'	C6'	C7'	178.1(8)	O2B	S1B	C1B	F2B	-63.8(7)
C5'	C6'	C7'	C8'	2.5(13)	O1B	S1B	C1B	F3B	-66.4(7)
C6'	C7'	C8'	C9'	-2.9(13)	O3B	S1B	C1B	F3B	170.9(6)
C6'	C7'	C8'	C10'	179.3(8)	O2B	S1B	C1B	F3B	53.5(7)
C12'	N2'	C9'	C8'	-0.2(13)	O2B'	S1B'	O1B'	O3B'	108.3(13)
Ru1	N2'	C9'	C8'	-178.7(7)	C1B'	S1B'	O1B'	O3B'	-69.8(17)
C12'	N2'	C9'	C4'	-178.7(8)	O2B'	S1B'	O3B'	O1B'	-107.4(12)
Ru1	N2'	C9'	C4'	2.8(10)	C1B'	S1B'	O3B'	O1B'	111.8(16)
C7'	C8'	C9'	N2'	-177.5(9)	O3B'	S1B'	C1B'	F3B'	120(2)
C10'	C8'	C9'	N2'	0.5(12)	O2B'	S1B'	C1B'	F3B'	7(3)
C7'	C8'	C9'	C4'	0.8(12)	O1B'	S1B'	C1B'	F3B'	-175(2)
C10'	C8'	C9'	C4'	178.9(8)	O3B'	S1B'	C1B'	F2B'	-8(2)
N1'	C4'	C9'	N2'	0.1(11)	O2B'	S1B'	C1B'	F2B'	-121(3)
C5'	C4'	C9'	N2'	-179.9(8)	O1B'	S1B'	C1B'	F2B'	57(2)
N1'	C4'	C9'	C8'	-178.3(8)	O3B'	S1B'	C1B'	F1B'	-121.3(19)
C5'	C4'	C9'	C8'	1.7(12)	O2B'	S1B'	C1B'	F1B'	126(3)

C9'	C8'	C10'	C11'	-0.7(13)	O1B'	S1B'	C1B'	F1B'	-56(2)
C7'	C8'	C10'	C11'	177.2(9)	O3A	S1A	O2A	C1A	88.7(17)
C8'	C10'	C11'	C12'	0.5(14)	O1A	S1A	O2A	C1A	-97.7(15)
C9'	N2'	C12'	C11'	0.0(13)	O2A	S1A	C1A	F1A	-51.4(11)
Ru1	N2'	C12'	C11'	178.5(7)	O3A	S1A	C1A	F1A	-168.3(13)
C9'	N2'	C12'	C13	-175.7(8)	O1A	S1A	C1A	F1A	60.6(14)
Ru1	N2'	C12'	C13	2.7(10)	O2A	S1A	C1A	F2A	71.4(11)
C10'	C11'	C12'	N2'	-0.2(14)	O3A	S1A	C1A	F2A	-45.5(15)
C10'	C11'	C12'	C13	174.7(9)	O1A	S1A	C1A	F2A	-176.7(12)
C17	N3	C13	C14	0.0(9)	O2A	S1A	C1A	F3A	-170.2(12)
Ru1	N3	C13	C14	-177.7(5)	O3A	S1A	C1A	F3A	72.9(13)
C17	N3	C13	C12	170.0(13)	O1A	S1A	C1A	F3A	-58.2(13)
Ru1	N3	C13	C12	-7.8(14)	O3A	S1A	C1A	O2A	-116.9(10)
C17	N3	C13	C12'	-178.1(6)	O1A	S1A	C1A	O2A	112.0(9)
Ru1	N3	C13	C12'	4.1(8)	S1A	O2A	C1A	F1A	131.8(11)
N2	C12	C13	N3	4(2)	S1A	O2A	C1A	F2A	-118.2(11)
C11	C12	C13	N3	178(2)	S1A	O2A	C1A	F3A	19(2)
N2	C12	C13	C14	172.9(13)	O3A'	S1A'	C1A'	F3A'	55.5(9)
C11	C12	C13	C14	-13(3)	O2A'	S1A'	C1A'	F3A'	179.0(8)
N2'	C12'	C13	N3	-4.2(10)	O1A'	S1A'	C1A'	F3A'	-58.2(8)
C11'	C12'	C13	N3	-179.4(9)	O3A'	S1A'	C1A'	F1A'	175.2(8)
N2'	C12'	C13	C14	177.9(7)	O2A'	S1A'	C1A'	F1A'	-61.4(10)
C11'	C12'	C13	C14	2.7(15)	O1A'	S1A'	C1A'	F1A'	61.5(8)
N3	C13	C14	C15	1.0(10)	O3A'	S1A'	C1A'	F2A'	-65.9(8)
C12	C13	C14	C15	-167.6(15)	O2A'	S1A'	C1A'	F2A'	57.6(10)
C12'	C13	C14	C15	178.7(8)	O1A'	S1A'	C1A'	F2A'	-179.6(7)
C13	C14	C15	C16	-1.5(11)	C3S	O1S	C1S	C2S	167(5)
C14	C15	C16	C17	0.8(11)	C1S	O1S	C3S	C4S	-169(7)
C14	C15	C16	C18	179.7(7)	C3S'	O1S'	C1S'	C2S'	177(7)
C13	N3	C17	C16	-0.7(8)	C1S'	O1S'	C3S'	C4S'	151(6)

Symmetry operations:

1 'x, y, z'; 2 '-x, y, -z+1/2'; 3 'x+1/2, y+1/2, z'; 4 '-x+1/2, y+1/2, -z+1/2'; 5 '-x, -y, -z'; 6 'x, -y, z-1/2'; 7 '-x+1/2, -y+1/2, -z'; 8 'x+1/2, -y+1/2, z-1/2'.